Analysis of isoform-specific tau aggregates suggests a common toxic mechanism involving similar pathological conformations and axonal transport inhibition

Kristine Cox [a,b,c], Benjamin Combs [a,b], Brenda Abdelmesih [b], Gerardo Morfini [b,d], Scott T. Brady [d,b], Nicholas M. Kanaan [a,e,f,*]

[a] Department of Translational Science and Molecular Medicine, Michigan State University, College of Human Medicine, Grand Rapids, MI, USA
[b] Marine Biological Laboratory, Woods Hole, MA, USA
[c] California National Primate Research Center, University of California, Davis, CA, USA
[d] Department of Anatomy and Cell Biology, University of Illinois at Chicago, Chicago, IL, USA
[e] Neuroscience Program, Michigan State University, East Lansing, MI, USA
[f] Hauenstein Neuroscience Center, Mercy Health Saint Mary's, Grand Rapids, MI, USA

ARTICLE INFO

ABSTRACT

Misfolded tau proteins are characteristic of tauopathies, but the isoform composition of tau inclusions varies by tauopathy. Using aggregates of the longest tau isoform (containing 4 microtubule-binding repeats and 4-repeat tau), we recently described a direct mechanism of toxicity that involves exposure of the N-terminal phosphatase-activating domain (PAD) in tau, which triggers a signaling pathway that disrupts axonal transport. However, the impact of aggregation on PAD exposure for other tau isoforms was unexplored. Here, results from immunochemical assays indicate that aggregation-induced increases in PAD exposure and oligomerization are common features among all tau isoforms. The extent of PAD exposure and oligomerization was larger for tau aggregates composed of 4-repeat isoforms compared with those made of 3-repeat isoforms. Most important, aggregates of all isoforms exhibited enough PAD exposure to significantly impair axonal transport in the squid axoplasm. We also show that PAD exposure and oligomerization represent common pathological characteristics in multiple tauopathies. Collectively, these results suggest a mechanism of toxicity common to each tau isoform that likely contributes to degeneration in different tauopathies.

© 2016 The Author(s). Published by Elsevier Inc. This is an open access article under the CC BY-NC-ND license (http://creativecommons.org/licenses/by-nc-nd/4.0/).

1. Introduction

A group of diseases collectively known as tauopathies are characterized by the accumulation of abnormal forms of the microtubule-associated protein called tau (Crowther and Goedert, 2000). In addition to Alzheimer's disease (AD), this group of diseases includes corticobasal degeneration (CBD), Pick's disease (PiD), progressive supranuclear palsy (PSP), frontotemporal dementia with parkinsonism linked to chromosome 17, and chronic traumatic encephalopathy (CTE), among others (Spillantini and Goedert, 2013). Each disease is characterized by pathognomonic tau inclusions, such as the neuronal neurofibrillary tangles, neuropil threads and neuritic plaques in AD, glial (astrocytic and oligoden-droglial) inclusions in CBD and PSP, neuronal Pick bodies in PiD, or mixed neuronal and glial inclusions in CTE (Kovacs, 2015; McKee et al., 2013; Yoshida, 2006). The clinical symptoms and affected brain regions further differentiate tauopathies. Interestingly, there is an apparent link between tau isoforms and different human tauopathies, as there is some degree of specificity for certain tau isoforms forming the pathognomonic tau inclusion of each disease (Kovacs, 2015).

In the adult human central nervous system, tau is normally expressed as 6 isoforms that are derived from alternative splicing of 3 exons (Wang and Mandelkow, 2016). Alternative splicing of exon 10, located in the second microtubule-binding repeat, gives rise to isoforms containing either 4 or 3 microtubule-binding repeat domains (4R or 3R, respectively). The 4R and 3R isoforms are further separated into 3 distinct isoforms that contain either exons 2 and 3, exon 2 only, or neither of these exons. Multiple studies provide

* Corresponding author at: Department of Translational Science and Molecular Medicine, Michigan State University, College of Human Medicine, 333 Bostwick Ave NE, Grand Rapids, MI 49503, USA. Tel.: (616) 234-0956; fax: (616) 234-0990.
E-mail address: Nicholas.kanaan@hc.msu.edu (N.M. Kanaan).

evidence that tau isoforms exhibit differing properties in terms of microtubule-binding affinity (Butner and Kirschner, 1991; Litersky et al., 1993; Trinczek et al., 1995; Voss and Gamblin, 2009), microtubule bundling (Chen et al., 1992; Kanai et al., 1989; Scott et al., 1992), regulation of microtubule dynamics (Bunker et al., 2004; Goedert and Jakes, 1990; Levy et al., 2005; Panda et al., 2003; Scott et al., 1991; Trinczek et al., 1995), levels of expression during development (Boutajangout et al., 2004; Goedert and Jakes, 1990; Hong et al., 1998) and/or aggregate formation in vitro (Adams et al., 2010; Combs et al., 2011; King et al., 2000; Voss and Gamblin, 2009; Zhong et al., 2012). However, the biological importance and disease relevance of each tau isoform remains relatively unclear. In the context of human disease, the pathology of AD and CTE is largely comprised of a mixture of 3R and 4R tau isoforms, the inclusions in CBD, PSP, and frontotemporal dementia with parkinsonism linked to chromosome 17 are primarily composed of 4R isoforms, and PiD pathology mostly contains 3R tau isoforms (Buee and Delacourte, 1999; Ferrer et al., 2014; Goedert et al., 1992; Munoz et al., 2003; Sergeant et al., 1999; Yoshida, 2006). Although these differences are well documented, the question of whether there are common or disease-specific mechanisms of toxicity for different misfolded tau isoforms remains unanswered.

Recently, our group identified inhibition of anterograde, kinesin-1-dependent fast axonal transport (FAT) as a toxic mechanism for disease-related forms of tau (Kanaan et al., 2013). Using the isolated squid axoplasm preparation, this toxic effect of tau was found to be mediated, at least in part, by pathological changes in tau conformation that expose an N-terminal motif termed the phosphatase-activating domain (PAD; Kanaan et al., 2011, 2012; LaPointe et al., 2009). Several modifications promoted aberrant PAD exposure, including phosphorylation, filament formation, and oligomerization. The latest is of particular interest because soluble prefibrillar tau aggregates appear to represent toxic forms of tau in several tauopathy models and may play a role in the spreading of tau pathology from cell-to-cell (Cardenas-Aguayo Mdel et al., 2014; Lewis and Dickson, 2016; Ward et al., 2012). The PAD in tau is involved in a signaling pathway whereby exposure of PAD activates protein phosphatase 1 (PP1), which in turn activates glycogen synthase kinase 3β (GSK3) via dephosphorylation of serine 9. Active GSK3 phosphorylates kinesin light chains causing cargo dissociation and disruption of fast anterograde axonal transport (Morfini et al., 2002). Previously, all studies demonstrating inhibition of axonal transport by pathogenic forms of tau have used the longest 4R tau isoform. Therefore, the question of whether aggregates of all 6 human isoforms oligomerize, display PAD, and inhibit axonal transport has not been evaluated. Such information would help to identify the extent to which PAD exposure contributes to toxicity in human tauopathies that display pathology comprised of different tau isoforms. In this work, we evaluated levels of PAD exposure, oligomer formation, and axonal transport toxicity for aggregates composed of each of the 6 human tau isoforms.

2. Materials and methods

2.1. Recombinant tau proteins

Six human isoforms of tau protein are created by alternative splicing in the adult central nervous system (Fig. 1A). Inclusion or exclusion of exon 10 creates 2 isoform categories that contain either 4 or 3 microtubule-binding repeat domains (i.e., 4R or 3R isoforms), respectively (Wang and Mandelkow, 2016). The 4R and 3R isoforms are further divided into 3 separate isoforms by alternative splicing of 2 N-terminal exons and contain either both (exons 2 and 3, 2N), 1 (exon 2, 1N), or 0 (neither exon 2 nor exon 3, 0N) of these exons. The isoform containing 2N4R is hT40 (441 amino acids), 1N4R is hT34 (412 amino acids), 0N4R is hT24 (383 amino acids), 2N3R is hT39 (410 amino acids), 1N3R is hT37 (381 amino acids), and 0N3R is hT23 (352 amino acids). All constructs were expressed in Escherichia coli using the pT7c plasmid and each contained a C-terminal 6× histidine tag for purification. DNA sequences were verified by sequencing before use in protein production. Recombinant proteins of each isoform were purified using immobilized metal affinity chromatography (Talon resin, 635502, Clontech) followed by size exclusion chromatography over an S200 column (26/60, 17-1195-01, GE Healthcare) using methods similar to those described (Carmel et al., 1994, 1996). Proteins (in 250-mM NaCl, 10-mM HEPES (4-(2-hydroxyethyl)-1-piperazineethanesulfonic acid), pH 7.4, 0.1-mM EGTA (ethylene glycol-bis(β-aminoethyl ether)-N,N,N',N'-
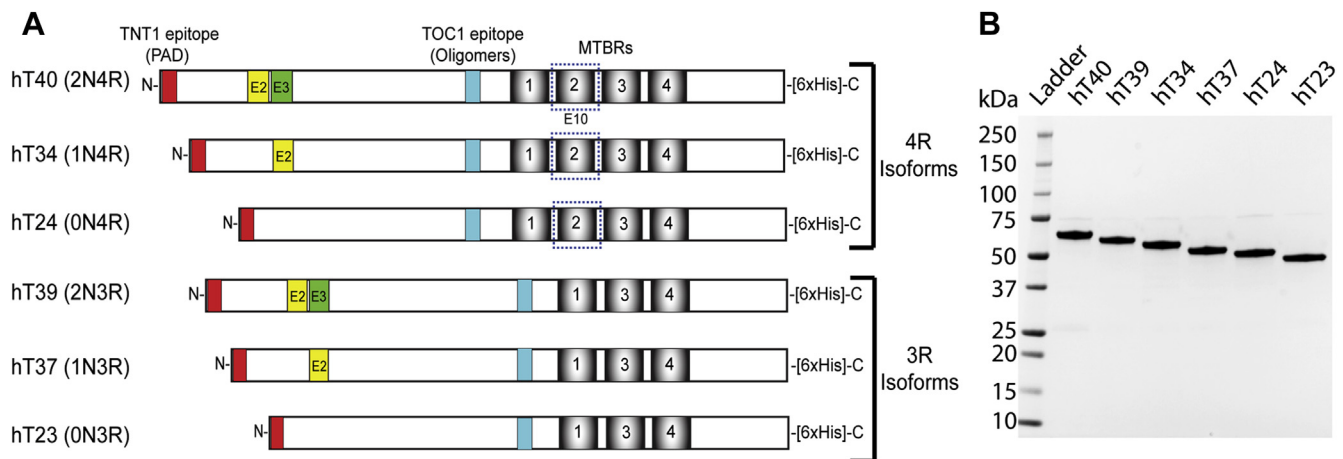
Fig. 1. Schematic of 6 human tau isoform proteins expressed in the adult central nervous system. (A) Each naturally occurring tau isoform is generated through alternative splicing of exons 2 (yellow), 3 (green), and 10 (within the second microtubule-binding regions [MTBR]). Each isoform contains the PAD epitope (red) corresponding to amino acids 2-18 and the tau oligomeric complex epitope (blue) mapped to amino acids 209-224 on hT40. There are 3 isoforms with 4 MTBRs, 1 with E2 and E3 (hT40, 2N4R, and 441 amino acids), E2 and not E3 (hT34, 1N4R, and 412 amino acids), and 1 with neither E2 nor E3 (ht24, 0N4R, and 383 amino acids). There are 3 isoforms with 3 MTBRs, 1 with E2 and E3 (hT39, 2N4R, and 410 amino acids), E2 and not E3 (hT37, 1N4R, and 381 amino acids), and 1 with neither E2 nor E3 (ht23, 0N4R, and 352 amino acids). (B) Each recombinant tau isoform protein was run in SDS-PAGE, and the gel was stained with Coomassie to show each protein (3 μg/lane) and demonstrate equivalent amounts of each protein used in our preparations. Abbreviation: PAD, phosphatase-activating domain. (For interpretation of the references to color in this figure legend, the reader is referred to the Web version of this article.)

tetraacetic acid), and 1-mM dithiothreitol) were quantified using an SDS (sodium dodecyl sulfate) Lowry protein assay.

The SDS Lowry was performed by adding bovine serum albumin (BSA) protein stock (2 mg/mL, 23,209, Thermo Scientific) or unknown, purified tau protein stocks to SDS solution (2% SDS, 5% β-mercaptoethanol, 10% glycerol, 62.5-mM Tris, pH 6.8) to a final volume of 100 μL. BSA protein standards of 0, 2, 4, 8, 16, and 32 μg were used, and blank samples without tau protein were used for the tau samples. The proteins were precipitated by adding 1 mL of 10% perchloric acid and/or 1% phosphotungstic acid to each sample and incubated 1 hour on ice. The samples were centrifuged at $18,000 \times g$ for 15 minutes at 4 °C, and the supernatant was removed. After air-drying the protein pellet, it was dissolved in 1 mL of Lowry solution (0.01% $CuSO_4$, 0.02% sodium potassium tartate, and 2% sodium carbonate in 0.1 N sodium hydroxide) and incubated at room temperature for 10 minutes. Then, 100 μL of Folin-Ciocalteu's phenol reagent (diluted 1:1 in water, F9252, Sigma-Aldrich) was added and incubated for 30—45 minutes at room temperature. Then, absorbance at 750 nm was measured using a spectrophotometer. Tau protein concentrations were interpolated from the BSA standard curve (linear regression, $r^2 = 0.994$). The protein was aliquoted into 10—50 μL and frozen at −80 °C until used in experiments outlined in the following sentences. Purified tau protein isoforms were visualized using SDS-PAGE and Coomassie staining (Fig. 1B) to confirm protein quality and consistency in protein assay results across the isoforms. It is noteworthy that this specific protein assay is routinely used by our group and produces consistent results in our hands.

2.2. In vitro tau polymerization reaction

Tau aggregation was induced with arachidonic acid (ARA; 90,010, Cayman Chemical) using methods similar to those previously described (Kanaan et al., 2012). Briefly, recombinant tau (2 μM) was incubated in polymerization buffer (5-mM dithiothreitol, 100-mM NaCl, 0.1-mM ethylenediaminetetraacetic acid, 10-mM HEPES, pH 7.6) with 75-μM ARA at room temperature for 6 hours. ARA was stored at −20 °C, and working solutions were prepared in 100% ethanol immediately before use. To obtain monomeric control samples, tau (2 μM) was prepared in polymerization buffer with ARA vehicle (ethanol), immediately aliquoted, and then stored at −80 °C. The extent of aggregation was determined using a combination of the right-angle laser light scatter (LLS) assay, thioflavin S (ThS) fluorescence, and transmission electron microscopy as described in the following paragraphs.

2.3. Right-angle LLS assay

A right-angle LLS system was used to measure the intensity of scattered light (I_S) as described in the study by Gamblin et al. (2000). Briefly, the system was composed of a 475-nm laser (BWI-475-20-E, B&W Tek, Inc), a high-sensitivity CMOS digital camera (DCC1240M, Thor Labs) and imaging software uc480 Viewer version 4.2. Images of scattered light were captured after 6 hours of polymerization at room temperature, a time at which a steady state of polymerization has been reached (Gamblin et al., 2000; Sarthy and Gamblin, 2006). Images were analyzed in Photoshop v12.1 (Adobe Systems) using the marquee tool to select a region of interest (75 × 10 pixels) within the scattered light band near the middle of the cuvette. The pre-ARA baseline I_S was subtracted from each post-ARA I_S measurement. Each experiment was repeated 4 independent times, and background-corrected intensity of I_S was used for comparisons.

2.4. ThS fluorescence assay

The formation of β-sheet structures was measured after 6 hours of polymerization at room temperature using a ThS fluorescence assay. A 0.0175% solution of ThS (T1892, Sigma) was prepared on the day of each experiment and cleared through a 0.22-μm filter before use. For each sample, 6 μL of ThS was added to 150 μL of 2-μM monomer or aggregated tau in a black 96-well plate (06-443-2, Fisher Scientific). After 20 minutes incubation at room temperature, fluorescence measurements were made using a Promega GloMax Multi Detection System with an excitation wavelength of 490 nm and an emission wavelength of 510—570 nm. Background fluorescence was measured in wells containing tau monomers with ARA vehicle (i.e., ethanol) and subtracted from each respective aggregate condition. Each experiment was repeated 4 independent times.

2.5. Transmission electron microscopy

Transmission electron microscopy was used to visualize the morphology of aggregates formed by each isoform after 6 hours of polymerization at room temperature as described in the study by Kanaan et al. (2012). A 10-μL aliquot of each 2-μM monomeric or polymerized tau sample was fixed with 2% glutaraldehyde (tau was 1.6-μM final concentration), spotted onto 300 mesh formvar carbon-coated copper grids (FCF300-Cu, Electron Microscopy Sciences), and negatively stained with 2% uranyl acetate. Grids were examined with a JEOL JEM-1400 Plus electron microscope at 80 kV and 10,000× magnification. Images were captured with an AMT XR81 digital camera and AMT software version 602.6 (Advanced Microscopy Techniques).

2.6. Soluble tau extraction from fresh-frozen human tissue

Fresh-frozen frontal cortex tissue from nondemented control, PiD, CBD, and AD cases (n = 4 per group) were obtained from the Brain Bank of the Cognitive Neurology and Alzheimer's Disease Center at Northwestern University. For detailed human subject information see Table S1. Soluble tau and sarkosyl-insoluble tau fractions were obtained as described previously in the study by Kanaan et al. (2016). Briefly, tissue pieces (0.5—1 g) were homogenized on ice in 10 volumes (1 g = 10 mL) of brain homogenization buffer (50-mM Tris pH 7.4, 274-mM NaCl, 5-mM KCl, 1-mM PMSF [phenylmethanesulfonyl fluoride], and 10 μg/mL each of pepstatin, leupeptin, bestatin, and aprotinin). The soluble tau fraction was collected in the supernatant after centrifugation at $27,000 \times g$ for 20 minutes at 4 °C. The following pellet was homogenized in brain pellet homogenization buffer (10-mM Tris pH 7.4, 800-mM NaCl, 10% sucrose, 1-mM EGTA, 1-mM PMSF) and centrifuged using same parameters as previously mentioned. The supernatant was collected, 1% sarkosyl (final concentration) was added, samples were incubated at 37 °C for 1 hour, and then centrifuged at $200,000 \times g$ for 1 hour at 4 °C. Then, the final pellet was resuspended in 1 mL of brain pellet homogenization buffer to obtain the sarkosyl-insoluble tau fraction. Both the soluble tau and sarkosyl-insoluble tau fractions were assayed for total protein concentration using the SDS Lowry protein assay and stored at −80 °C until used in sandwich ELISAs for analysis (see in the following paragraphs).

2.7. Antibodies

Four tau antibodies were used in this study to characterize aggregates composed of each tau isoform. The Tau5 antibody (mouse monoclonal IgG1, Binder/Kanaan Lab) recognizes aa 210-230

(Carmel et al., 1996) and is unaffected by phosphorylation or conformation. The TNT1 antibody (mouse monoclonal IgG1, Binder/Kanaan Lab) was made against PAD (i.e., amino acids 2-18 and epitope between 7 and 12) and is a useful marker of PAD exposure in nondenaturing assays (Combs et al., 2016; Kanaan et al., 2012, 2016). The TOC1 antibody (mouse monoclonal IgM, Binder/Kanaan Lab) has an epitope between 209 and 224 and selectively recognizes oligomeric tau aggregates compared with monomeric or filamentous aggregates (Patterson et al., 2011a; Ward et al., 2013). The R1 antibody (Binder Lab) is a rabbit polyclonal pan-tau antibody with numerous epitopes throughout the tau protein (Berry et al., 2004).

2.8. Tau sandwich enzyme-linked immunosorbent assays

Sandwich enzyme-linked immunosorbent assays (ELISAs) were used to measure the relative levels of total tau, PAD-exposed tau, and oligomeric tau in recombinant tau protein samples and tau isolated from the frontal cortex of human brains (Kanaan et al., 2016). All steps were performed at room temperature. Wells were washed between each step using 200 μL/well of ELISA wash buffer (100-mM borate acid, 25-mM sodium borate, 75-mM NaCl, 0.25-mM thimerosal, 0.4% [w/v] bovine serum albumin, 0.05% [v/v] Tween-20), and 50 μL solution per well was used for all other steps.

For sandwich ELISAs with recombinant tau samples, Tau5 (2 μg/mL), TNT1 (2 μg/mL), or TOC1 (2 μg/mL) capture antibodies were diluted in borate saline (100-mM borate acid, 25-mM sodium borate, 75-mM NaCl, and 0.25-mM thimerosal) and applied at 50 μL solution per well to coat high-binding 96-well microplates (catalog #07-200-35, Fisher Scientific) for 60 minutes. Plates were washed twice with ELISA wash buffer, and then blocked for 60 minutes with ELISA wash containing 5% nonfat dry milk (block solution). Two washes were performed, and then recombinant tau samples were added to each well for 90 minutes. Tau monomers or aggregates from the in vitro polymerization assays were diluted with polymerization buffer to a final concentration of 5 nM (Tau5 assays), 100 nM (TNT1 assays), or 150 nM (TOC1 assay). Titer assays for each version of the sandwich ELISA were performed to ensure assays were within the linear range. Wells were rinsed 3 times and then incubated with R1 diluted 1:20,000 (50 ng/mL) in block solution for 90 minutes, to serve as the detection antibody. Wells were washed 3 times, and then incubated for 60 minutes with goat anti-rabbit IgG conjugated to horseradish peroxidase (1:5000; PI-2000, Vector Labs) diluted in block solution. Wells were washed 3 times, and assays were developed using 3,3′,5,5′-tetramethylbenzidine (TMB; T0440, Sigma) for 20 minutes (Tau5 and TNT1 assays) or 35 minutes (TOC1 assay). The reactions were stopped with 3.5% sulfuric acid, and absorbance was read at 450 nm on a SpectraMax Plus 384 microplate reader (Molecular Devices). The amount of total tau applied in the assay was known and equivalent between groups since purified recombinant protein samples were used, but absorbance (A) is not linear (i.e., $A = Log_{10}(1/transmittance)$) and not useful for comparing across samples. Thus, the absorbance data were converted to percent absorbed light (a linear scale) using the following equation $\%A = (1-10^{-x})*100$, where x is absorbance. Since R1 is a polyclonal anti-tau antibody, the percent light absorbed data from the TNT1 and TOC1 assays were normalized to the data from the Tau5 assays (i.e., total tau levels) to account for any R1-based detection variations with different tau isoforms. The normalized data were used for statistical comparisons across groups.

The same protocol was used to measure the levels of total tau, PAD exposure and tau oligomers in soluble and sarkosyl-insoluble tau fractions of the frontal cortex from control, PiD, CBD, and AD brains (n = 4 per group; Table S1). All steps were identical with the exception that human brain samples were used. The samples were diluted to a final total protein concentration of 0.4 μg/μL (i.e., 20 μg/well) for soluble tau fractions or 0.08 μg/μL (i.e., 4 μg/well) for insoluble tau fractions. The protein amount was determined in titer experiments to ensure the ELISAs were performed within the linear rage. Tau standard ELISAs were performed simultaneously with human sample sandwich ELISAs to estimate the amount of tau captured by Tau 5, TNT1 or TOC1, and detected with R1. A serial dilution of recombinant hT40 monomer (ranging from 250 to 1.0 ng/well) was bound to the ELISA plate for 60 minutes, then blocked as previously mentioned, and detection was performed using R1, and then the horseradish peroxidase-secondary antibody exactly as in the sandwich ELISAs. Each standard was run in duplicate and developed simultaneously with the sandwich ELISAs to ensure accurate interpolation of unknown tau amounts. The standard curve data were log_{10} transformed and best fit to a sigmoidal curve ($r^2 = 0.998$). This provided a standard curve of absorbance values that were derived from R1 reactivity with known amounts of tau protein. The quantity of tau (ng) in each human sample was interpolated from the tau standard curves and then converted to a concentration of ng/μL by dividing the interpolated quantity by the volume of the sample used (i.e., 50 μL). Finally, the data (i.e., concentrations of tau) were normalized to reduce skewness using logarithmic transformations and then used for statistical comparisons.

2.9. Immunoblotting

Monomeric and aggregated tau samples were prepared in Laemmli sample buffer (20-mM Tris pH 6.8, 6% glycerol [v/v], 1.6% sodium dodecyl sulfate [v/v], 0.85% 2-mercaptoethanol [v/v], 0.002% Bromophenol blue [v/v]), incubated at 90 °C for 5 minutes, separated by SDS-PAGE using 4%—20% Criterion TGX precast gels (5671094, Bio-Rad Laboratories) and transferred to 0.22-μm nitrocellulose membranes (66,485, Pall Corporation, Pensacola, FL, USA). Membranes were blocked with 2% nonfat dry milk in Tris-buffered saline (TBS; 50-mM Tris, 150-mM NaCl, pH 7.4), and incubated overnight at 4 °C in Tau5 (1:100,000), TNT1 (1:300,000), or TOC1 (1:5000). Membranes were rinsed in TBS + 0.1% Tween 20 and developed with the goat anti-mouse IgG (H+L) IRDye 680LT secondary antibody (1:20,000; 926-68,020, LiCor) for TNT1 blots, or goat anti-mouse IgG (H+L) IRDye 800LT secondary antibody (1:20,000; 926-68,020, LiCor) for Tau5 and goat anti-mouse IgM IRDye 680LT secondary antibody (1:20,000; 926-68,080, LiCor) for TOC1 blots. Image acquisition and intensity measurements were performed using a LiCor Odyssey system.

To confirm the preferential involvement of specific tau isoforms in different tauopathy pathologies, the insoluble tau fractions were processed for isoform identification on Western blots. Samples of sarkosyl-insoluble tau fractions (50 μL) were solubilized in a 6-M guanidine-HCl for 1.5 hours at room temperature and then dialyzed (3500 Da cutoff, #69550, Pierce) against TBS (pH 7.4) overnight at 4 °C. The resultant samples were precipitated using 10% trichloroacetic acid for 2 hours on ice, followed by centrifugation at 14,000 × g at 4 °C for 30 minutes. The pellets were washed with −20 °C acetone, centrifuged again at 14,000 × g for 20 minutes, and air-dried before resuspending in 40 μL of 1× FastAP Buffer (10-mM Tris-HCl, pH 8.0, 5-mM MgCl₂, 100-mM KCl, 0.02% Triton X-100, and 100 μg/mL BSA), then sonicated, and then dephosphorylated by adding 4-μL FastAP thermosensitive alkaline phosphatase (#EF0651, Thermo Scientific) and incubating at 37 °C for 1.5 hours. After dephosphorylation, 20 μL of 6× Laemmli sample buffer was added, and the samples were prepared as previously mentioned for separation on 10% TGX criterion gels (#5671033, BioRad) and transferred to nitrocellulose as previously mentioned. Due to proteolytic processing of the termini of tau proteins within

inclusions in tauopathies, we probed the membranes simultaneously with a combination of monoclonal mouse IgG1 antibodies with epitopes covering the protein: Tau13 is an N-terminal monoclonal antibody (epitope between aa8-9/13-21 [Combs et al., 2016]), Tau5 is a midtau monoclonal antibody (epitope between aa 210-230 [Carmel et al., 1996]) and Tau7 is a C-terminal monoclonal antibody (epitope between aa 430-441 [Horowitz et al., 2006]). The signal was detected using goat anti-mouse IgG1 IRDye 680LT secondary antibody (1:20,000; 926-68,050, LiCor) and imaged as previously mentioned.

2.10. Squid axoplasm motility assay

FAT was measured in freshly extruded squid axoplasm (*Loligo pealei*; Marine Biological Laboratory, Woods Hole, MA, USA) as previously described (Kanaan et al., 2011, 2012; LaPointe et al., 2009). Recombinant tau samples (monomer or aggregate) were diluted in X/2 buffer (175-mM potassium aspartate, 65-mM taurine, 35-mM betaine, 25-mM glycine, 10-mM HEPES, 6.5-mM $MgCl_2$, 5-mM EGTA, 1.5-mM $CaCl_2$, 0.5-mM glucose, 10-mM adenosine triphosphate, and pH 7.2) and perfused into isolated axoplasm at a final concentration of 2 μM (physiological range of tau; Alonso et al., 1996; King et al., 1999). Motility was analyzed using a Zeiss Axiomat microscope equipped with a 100× (1.3 numerical aperture) objective and differential interference contrast optics. Images were acquired using a Model C2400 CCD through a Hamamatsu Argus 20 and further process using a Hamamatsu Photonics Microscopy C2117 video manipulator for image adjustment and generation of calibrated cursors and scale bars. The rate of anterograde and retrograde FAT was measured by matching calibrated cursor movements to the speed of vesicles moving in the axoplasm over 50 minutes, and data were plotted as a function of time (Song et al., 2016). The average velocity of transport over the last 20 minutes of the assay was compared between monomer and aggregates of each isoform.

2.11. Triple-label immunofluorescence for confocal microscopy

Triple-label immunofluorescence (IF) was used to characterize the colocalization between PAD exposure (TNT1), oligomers (TOC1), and total tau pathology (R1). Most important, the sections were fixed with paraformaldehyde, a small molecule cross-linker, that does not readily disrupt protein structure (Mason and O'Leary, 1991; Rait et al., 2004), and the fixed, free-floating sections were not exposed to denaturants (e.g., heat or alcohols), to allow conformational differences to remain intact in the tissue sections. Tissue sections from age-matched, nondemented controls (n = 3), CBD (n = 4), PiD (n = 4), and AD cases (n = 3; Table S1) were processed for triple-label IF using the TNT1 (mouse IgG1), TOC1 (mouse IgM), and R1 (rabbit) antibodies according to published methods (Kanaan et al., 2016). The sections were incubated overnight at 4 °C in a primary antibody solution containing TNT1 (1:30,000), TOC1 (1:2000), and R1 (1:2500) antibodies followed by incubation in a secondary antibody solution of Alexa Fluor 488 goat anti-mouse IgG1-specific (A-21121, Invitrogen), Alexa Fluor 568 goat anti-mouse IgM-specific (A-21043, Invitrogen), and Alexa Fluor 647 goat anti-rabbit specific (A-21244, Invitrogen) antibodies (all diluted 1:500) for 2 hours. Following the staining procedure, sections were mounted on microscope slides, autofluorescence was blocked using 2% sudan black, and the sections were coverslipped using hardset Vectashield mountant. Control sections with 1 of the 3 primary antibodies omitted confirmed that each secondary label was specific to the appropriate primary antibody (i.e., no staining was observed with the fluorophore for the omitted antibody; Fig. S1A—L). A Nikon A1+ laser scanning confocal

microscope system equipped with solid-state lasers (488, 561, and 640), and Nikon Elements AR software were used to acquire image z-stacks (0.5-μm step size), and the images (maximum intensity projections) were prepared for publication using Adobe Photoshop and Illustrator.

2.12. Statistics

All experiments were repeated at least 3 independent times. The data were assessed for meeting normality and equal variance assumptions using the D'Agostino-Pearson normality test and the Brown-Forsythe variance test, and when both were not met, the data were analyzed using nonparametric statistical tests (as indicated in the following sentences). In the recombinant tau protein experiments, normality tests were run by combining the 4R monomers (n = 12), 4R aggregates (n = 12), 3R monomers (n = 12), and 3R aggregates (n = 12) to obtain large enough sample sizes for better measuring normality. The human brain lysate data were log transformed to normalize the data as described previously. Experiments were analyzed by Student's *t*-test or Mann—Whitney test, with a 1-way analysis of variance (ANOVA) or Kruskal—Wallis test, or with a 2-way ANOVA as indicated in the results and figure legends. When overall significance was achieved, the Holm—Sidak post-hoc test (for ANOVAs) or the Dunn post-hoc test (for Kruskal—Wallis) was used to make all possible comparisons. Data were expressed as mean ± standard error of mean. All tests were two-tailed, and significance was set at $p \leq 0.05$. GraphPad Prism 6 software (GraphPad Software, Inc, LaJolla, CA, USA) was used for all statistical tests.

3. Results

3.1. In vitro aggregation of tau isoforms

Recombinant proteins corresponding to all tau isoforms were expressed in bacteria (Fig. 1B) and induced to aggregate in vitro at near physiological levels (i.e., 2 μM) using ARA (Alonso et al., 1996; King et al., 1999). Three well-established assays were used to measure the extent of tau isoform aggregation. Right-angle laser light scattering showed significantly greater scattered light intensity in all 4R tau isoforms when compared to 3R isoforms (1-way ANOVA with Holm—Sidak post-hoc, $F_{(5, 18)} = 60.22$, $p < 0.0001$; Fig. 2A). hT40 showed the highest amount of light scattering compared to other 4R isoforms, and there were no differences between the different 3R isoforms. Similar results were seen in the ThS assay, where the 4R isoforms were significantly higher than 3R isoforms (1-way ANOVA with Holm—Sidak post-hoc, $F_{(5, 18)} = 19.99$, $p < 0.0001$; Fig. 2B), and no differences were found in comparisons between the individual 4R isoforms or between the 3R isoforms. Interestingly, 4R tau isoforms formed morphologically distinct aggregates compared to 3R isoforms (Fig. 2C—H). A mixture of long, intermediate, and short filaments, as well as globular oligomers was present in 4R isoform reactions (Fig. 2C—E). In contrast, 3R isoforms were primarily composed of globular oligomers, and only very rare long filaments were found (Fig. 2F—H). Monomer samples were imaged to confirm the lack of aggregation, and as expected, the grids did not contain any aggregates (data not shown).

3.2. PAD exposure and oligomerization of tau isoforms

Nondenaturing sandwich ELISAs (Kanaan et al., 2016) were used to determine the levels of PAD exposure (TNT1 reactivity) in the isoform samples (Fig. 3A). The monomer groups were not normally distributed and did not display equal variance, thus nonparametric
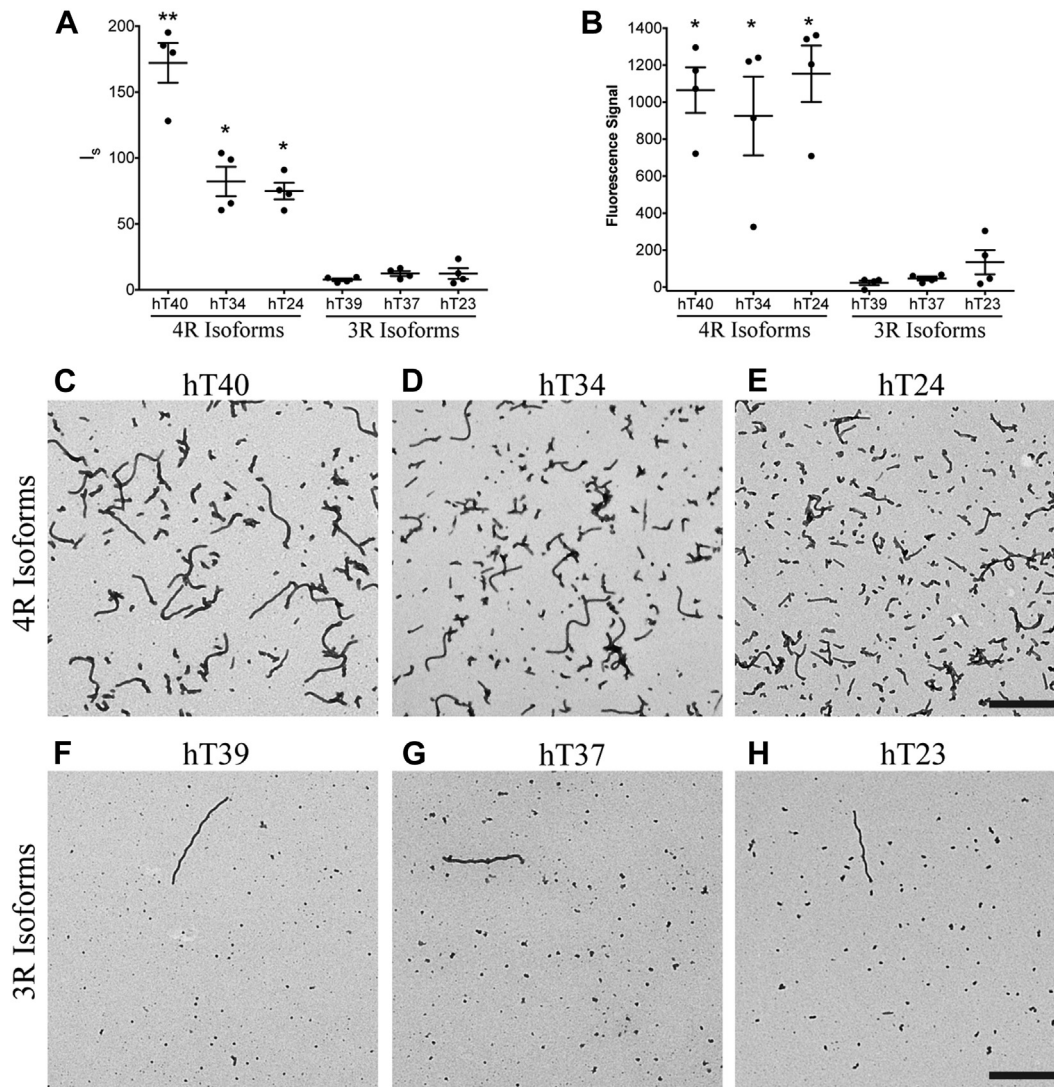
Fig. 2. Characterization of 4R and 3R isoform aggregation induced by arachidonic acid in vitro. (A) After 6 hours of polymerization, scattered laser light signal (I_s) from all three 4R isoforms is significantly greater than the 3R isoforms. Among the 4R isoforms, hT40 signal was significantly higher than hT34 and hT24, and within the 3R isoforms, all 3R constructs produced similar light scattering (one-way ANOVA, Holm-Sidak post-hoc comparisons: **$p < 0.05$ versus hT40 all other groups and *$p < 0.05$ versus all 3R isoforms, n = 4 per group). (B) Thioflavin S (ThS) fluorescence, a marker for β-sheet structures in aggregated tau, was significantly higher in all 4R tau isoforms compared with each 3R isoform. No differences were found between the different 4R or between the different 3R tau isoforms (one-way ANOVA, Holm−Sidak post-hoc comparisons: *$p < 0.05$ versus all 3R isoforms, n = 4 per group). All graphed values represent mean ± SEM. (C−H) Representative electron micrographs of hT40 (C), hT34 (D), hT24 (E), hT39 (F), hT37 (G), and hT23 (H) aggregates polymerized in the presence of arachidonic acid. The 4R tau isoforms formed a range of short, intermediate, and longer filaments compared with 3R tau isoforms, which formed mostly globular oligomeric aggregates and only rare filaments. Scale bar = 600 nm (applies to all panels). Abbreviations: ANOVA, analysis of variance; SEM, standard error of mean.

tests were used for comparisons including monomers. Comparisons between isoform monomers showed that hT39 monomer signal was significantly higher than hT24 and hT23 monomers (Kruskal−Wallis ANOVA with Dunn's post-hoc, H = 18.4, $p = 0.0025$). The hT24 aggregates showed the highest TNT1 signal, which reached significance compared with hT40, hT39, hT37, and hT23 aggregates (1-way ANOVA with Holm−Sidak post-hoc, $F_{(5, 18)} = 19.11$, $p < 0.0001$). Aggregates of all 6 tau isoforms showed significant increases in TNT1 reactivity when compared with their respective monomer samples (Fig. 3A; Mann−Whitney test, for all comparisons $p = 0.029$).

Sandwich ELISAs were used to determine the levels of tau oligomers (TOC1 reactivity) in the isoform samples (Fig. 3B). The monomer groups were not normally distributed and did not display equal variance, thus nonparametric tests were used for comparisons including monomers. Comparisons between isoform monomers showed that hT39 monomer signal was significantly higher

than hT24 and hT23 monomers (Kruskal−Wallis ANOVA with Dunn's post-hoc, H = 18.6, $p = 0.0023$). The hT24 aggregates showed the highest TOC1 signal, which reached significance compared with hT40, hT39, hT37, and hT23 aggregates, while hT34 aggregates were significantly different from hT39, hT37, and hT23 aggregates, and both hT40 and hT39 aggregates are significantly higher than hT37 and hT23 (1-way ANOVA with Holm−Sidak post-hoc, $F_{(5, 18)} = 50.77$, $p < 0.0001$). Aggregated samples for all 6 isoforms showed significant increases in TOC1 reactivity when compared with their respective monomer samples (Fig. 3B; Mann−Whitney tests, for all comparisons $p = 0.029$).

The same samples were denatured and run in SDS-polyacrylamide gel electrophoresis (PAGE) and Western blotting to confirm that the differences TNT1 and TOC1 reactivity were conformation-dependent. As expected, monomer and aggregated samples of all 6 tau isoforms showed equal reactivity for TNT1 and TOC1 when the samples were denatured because this exposes the
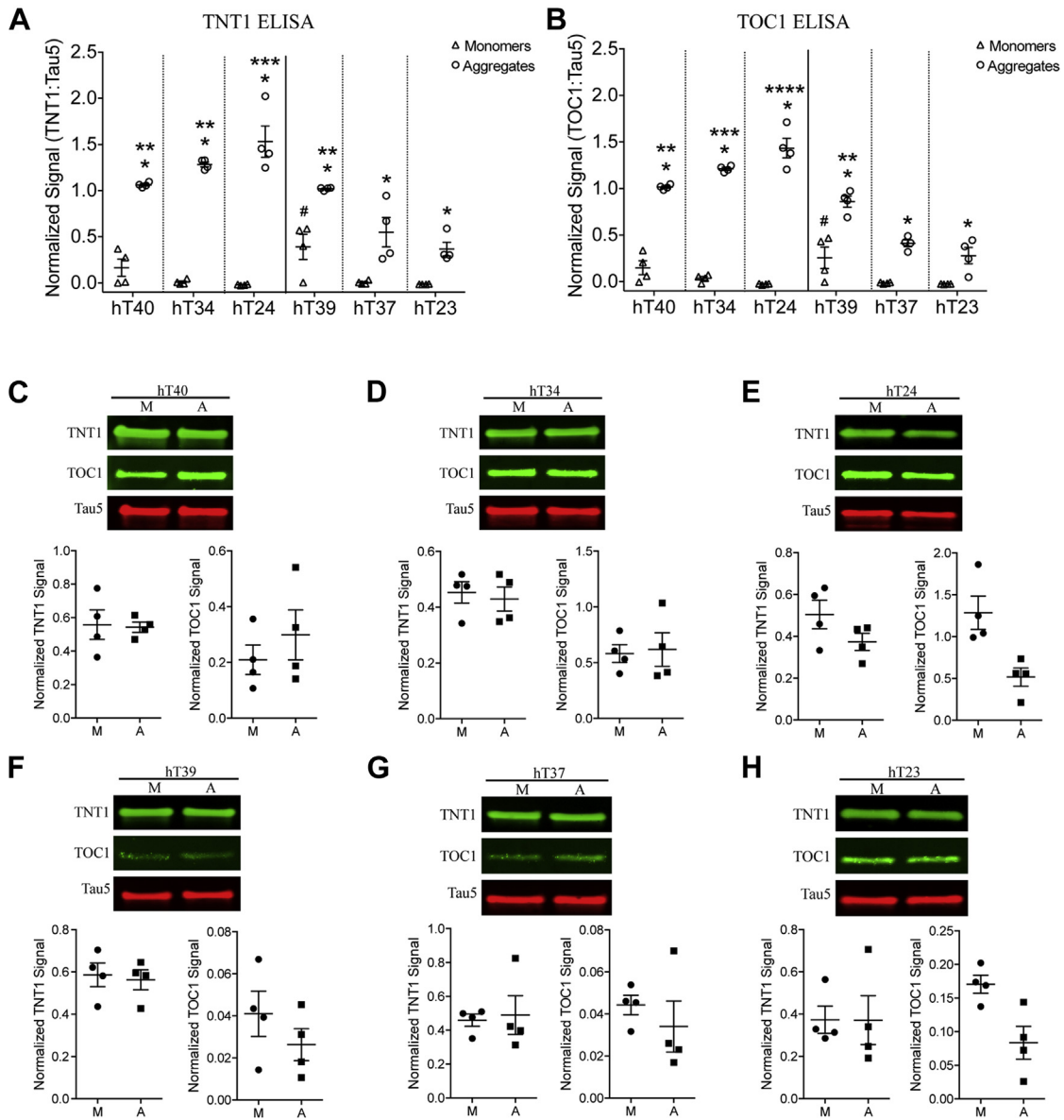
Fig. 3. Biochemical analysis of PAD exposure and oligomerization for all tau isoforms. (A, B) Sandwich ELISAs were used as nondenaturing assays to capture PAD-exposed tau (A, TNT1 capture antibody) and tau oligomers (B, TOC1 capture antibody), with detection of captured tau using the rabbit pan-tau antibody, R1. (A) The TNT1 ELISAs show significantly higher signal in aggregated samples compared with monomeric samples for each tau isoform. TNT1 signal was the highest in hT24 aggregates, which reached significance compared with hT40, hT39, hT37, and hT23 aggregates. hT40, hT34, and hT39 aggregates were significantly higher when compared with hT37 and hT23 aggregates. hT39 monomers were significantly different compared with hT34, hT24, hT37, and hT23 monomers. (B) Similarly, the TOC1 ELISAs show significantly higher signal in aggregated samples compared with monomeric samples for each tau isoform. TOC1 signal was the highest in hT24 aggregates, which reached significance when compared with hT40, hT39, hT37, and hT23 aggregates. hT40 and hT39 aggregates were significantly greater than hT37 and hT23 aggregates, while hT34 aggregates were significantly higher when compared hT39, hT37, and hT23. hT39 monomers were significantly different compared with hT24, hT37, and hT23 monomers. The data were compared using the Kruskal–Wallis ANOVA with Dunn post-hoc (isoform monomers), one-way ANOVA with Holm–Sidak post-hoc (isoform aggregates), and the Mann–Whitney test (monomers vs. aggregates). *$p < 0.05$ versus the monomer of the same isoform; **$p < 0.05$ versus hT37 and hT23 aggregates; ***$p < 0.05$ versus hT40, hT39, hT37, and hT23 aggregates; #$p < 0.05$ versus hT24 and hT23 monomers. (C–H) The same samples that were used for sandwich ELISAs were analyzed using SDS-PAGE and/or Western blotting as a denaturing assay (5 μL of 2-μM sample loaded in each lane). In TNT1 and TOC1 blots, the monomer and aggregate samples produced equal signal (Tau5 was used to normalize TNT1 and TOC1 signals, Student's *t*-test, all $p > 0.05$) because denaturation of the proteins exposes the epitopes making them equally accessible. Collectively, these data indicate that all tau isoforms have PAD exposed and form oligomers when induced to aggregate in vitro, and TNT1 and TOC1 strongly label aggregated forms of all tau isoforms, not monomers, in a conformation-dependent manner. Abbreviations: ANOVA, analysis of variance; ELISA, enzyme-linked immunosorbent assays; PAD, phosphatase-activating domain; SEM, standard error of mean.

epitopes making them equally accessible (Student's *t*-tests, for all comparisons $p > 0.05$; Fig. 3C–H).

3.3. Tau isoform aggregates inhibit FAT in isolated squid axoplasm

The effect of isoform-specific tau aggregates on FAT was evaluated using the isolated squid axoplasm model system as in our prior studies (Kanaan et al., 2011, 2012; LaPointe et al., 2009).

The anterograde FAT data were compared using a 2-way ANOVA, and overall significance was achieved for both factors (tau isoforms: $F_{(5,36)} = 4.487, p = 0.003$; and tau species: $F_{(1,36)} = 66.21, p < 0.0001$) but not the interaction ($F_{(5,36)} = 0.859, p = 0.518$). Perfusion of hT40, hT34, and hT24 aggregates into squid axoplasms significantly impaired anterograde transport (Fig. 4A) when compared with the respective monomers (all at 2 μM). Similarly, perfusion of squid axoplasms with hT39, hT37, and hT23 aggregates significantly
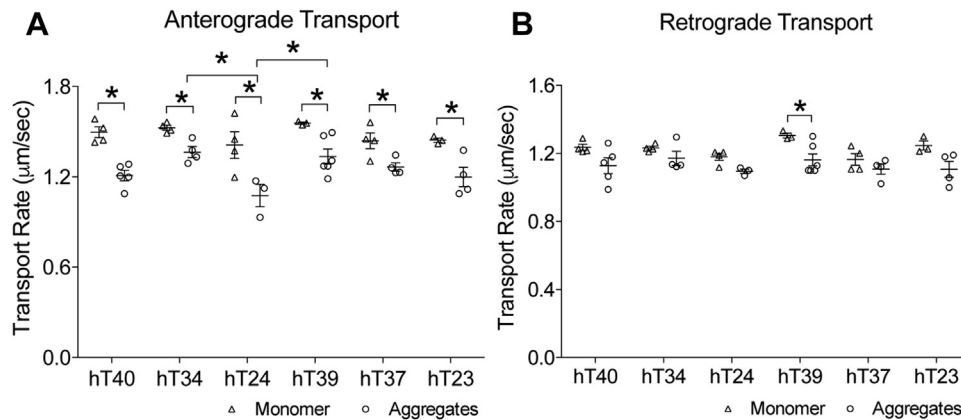
Fig. 4. Aggregates of all 6 tau isoforms significantly inhibit anterograde fast axonal transport (FAT) in the isolated squid axoplasm. (A, B) Squid axoplasms were perfused with each tau isoform (2 μM) in monomeric or aggregated forms, and FAT rates in both anterograde and retrograde directions were measured. (A) Quantification of average anterograde FAT rates during the last 20 minutes of the squid axoplasm assay indicate that aggregated forms of all 6 tau isoforms significantly inhibit anterograde FAT when compared with monomeric proteins. The strongest inhibitory effect was seen with hT24 aggregates, which reached statistical significance compared with hT34 and hT39 aggregates. (B) hT40, hT34, hT24, hT37, and hT23 aggregates did not significantly impair retrograde FAT when compared with monomers of the same isoform. Interestingly, hT39 aggregates caused a mild inhibition of retrograde FAT, compared with hT39 monomers, an effect not been observed with any other tau construct tested to date. All differences between groups were compared using a 2-way ANOVA with a Holm−Sidak post-hoc test ($^*p \leq 0.05$).

impaired anterograde FAT (Fig. 4A) when compared with the respective monomers (all at 2 μM). Pairwise comparisons within tau species showed that hT24 aggregates produced significantly more inhibition of anterograde FAT when compared to hT34 and hT39 aggregates. The retrograde FAT data were compared using a 2-way ANOVA, and overall significance was achieved for tau species ($F_{(1,36)} = 23.68$, $p < 0.0001$) but not for tau isoforms ($F_{(5,36)} = 2.269$, $p = 0.068$) or the interaction ($F_{(5,36)} = 0.582$, $p = 0.714$). hT40, hT34, hT24, hT37, and hT23 aggregates did not significantly impair retrograde FAT when compared to the respective monomers, but hT39 aggregates elicited a mild inhibitory effect on retrograde FAT (Fig. 4B). However, this effect appeared due to a slightly higher retrograde rate for hT39 monomer rather than a lower retrograde rate with hT39 aggregates. Plots of FAT rates over time of squid axoplasms incubated with monomeric and aggregated forms of each tau isoform are provided in Fig. S2. Collectively, these studies indicate that inhibition of anterograde FAT represents a toxic effect common to all tau aggregates, regardless of isoform composition.

### 3.4. PAD exposure and oligomers in human tauopathies

Tissue sections from tauopathy cases were stained using multilabel IF for TNT1 (PAD exposure), TOC1 (tau oligomers), and R1 (pan-tau marker) to confirm whether these modifications coexist in multiple tauopathies with pathologies spanning all of the tau isoforms. Cognitively unimpaired Braak stage I−II cases were used to establish whether these modifications coexist in the early stages of tau pathology deposition. Indeed, early pretangle neurons within the hippocampus were labeled with all antibodies in Braak I−II cases (Fig. 5A−D). In severe AD cases (i.e., Braak stage V−VI), all markers continue to colocalize in classic NFTs within the hippocampus that characterize AD tau pathology (Fig. 5E−H). In CBD, the characteristic astrocytic pathology (e.g., astrocytic plaques) showed extensive colocalization between TNT1, TOC1, and R1 in the frontal cortex (Fig. 5I−L). Similarly, the characteristic Pick bodies in the frontal cortex were well labeled by TNT1, TOC1, and R1 in PiD tissue (Fig. 5M−P). While the amount of overlap was extremely high in all cases, there were a small number of examples in which immunoreactivity for the 2 epitopes could be seen separately. In general, the remarkable colocalization between TNT1, TOC1, and R1 in all

tauopathies confirms that PAD exposure and tau oligomerization occur simultaneously in cells displaying tau pathology, irrespective of isoform composition.

We confirmed the isoform composition of pathology in the human tauopathy lysate samples using the sarkosyl-insoluble fractions. The AD, PiD, and CBD samples were solubilized in guanidine and dephosphorylated before running in Western blots (Fig. 6A). The band patterns in the immunoblots showed that the AD cases contained a mixture of isoforms, the PiD cases clearly contained 3R isoforms but also some 4R isoforms, while the vast majority of pathology in CBD cases was comprised of 4R tau isoforms. A recombinant protein standard containing all 6 human tau isoforms was run simultaneously to confirm that each isoform band was appropriately identified in the human samples.

Sandwich ELISAs were used to further evaluate whether there are differences in tau oligomerization and PAD exposure specifically between AD, CBD, and PiD cases. Total tau levels in the soluble fractions were similar for AD, CBD, and PiD, as indicated by the Tau5 sandwich ELISA (Fig. 6B; 1-way ANOVA, $F_{(2,9)} = 3.283$, $p = 0.085$). In contrast, AD soluble tau displayed the highest level of TNT1 followed by CBD, with PiD having the lowest levels (Fig. 6C; 1-way ANOVA with Holm−Sidak post-hoc, $F_{(2,9)} = 24.87$, $p = 0.0002$). Similarly, the soluble fraction from AD contained the greatest level of TOC1 reactivity, followed by CBD, and then PiD had the lowest signal (Fig. 6D; 1-way ANOVA with Holm−Sidak post-hoc, $F_{(2,9)} = 16.57$, $p = 0.001$). As a point of reference, the levels of total tau, TOC1, and TNT1 for ND control cases are provided as dashed line (data not shown). Total tau levels in the insoluble fractions, as detected by Tau5, were the highest in AD, followed by CBD and PiD contained the least (Fig. 6E; 1-way ANOVA with Holm−Sidak post-hoc, $F_{(2,9)} = 25.93$, $p = 0.0002$). TNT1 detected significantly more PAD-exposed tau in AD compared with PiD, and more in CBD when compared with PiD, but AD and CBD were not different (Fig. 6F; 1-way ANOVA with Holm−Sidak post-hoc, $F_{(2,9)} = 12.07$, $p = 0.0028$). TOC1 detected significantly more oligomeric tau in AD compared to CBD and PiD and more in CBD compared with PiD (Fig. 6G; 1-way ANOVA with Holm−Sidak post-hoc, $F_{(2,9)} = 35.32$, $p < 0.0001$). These data complement our findings from the IF studies using fixed tissue sections (Fig. 5) and further support the co-occurrence of tau oligomerization and PAD exposure in AD, CBD, and PiD.
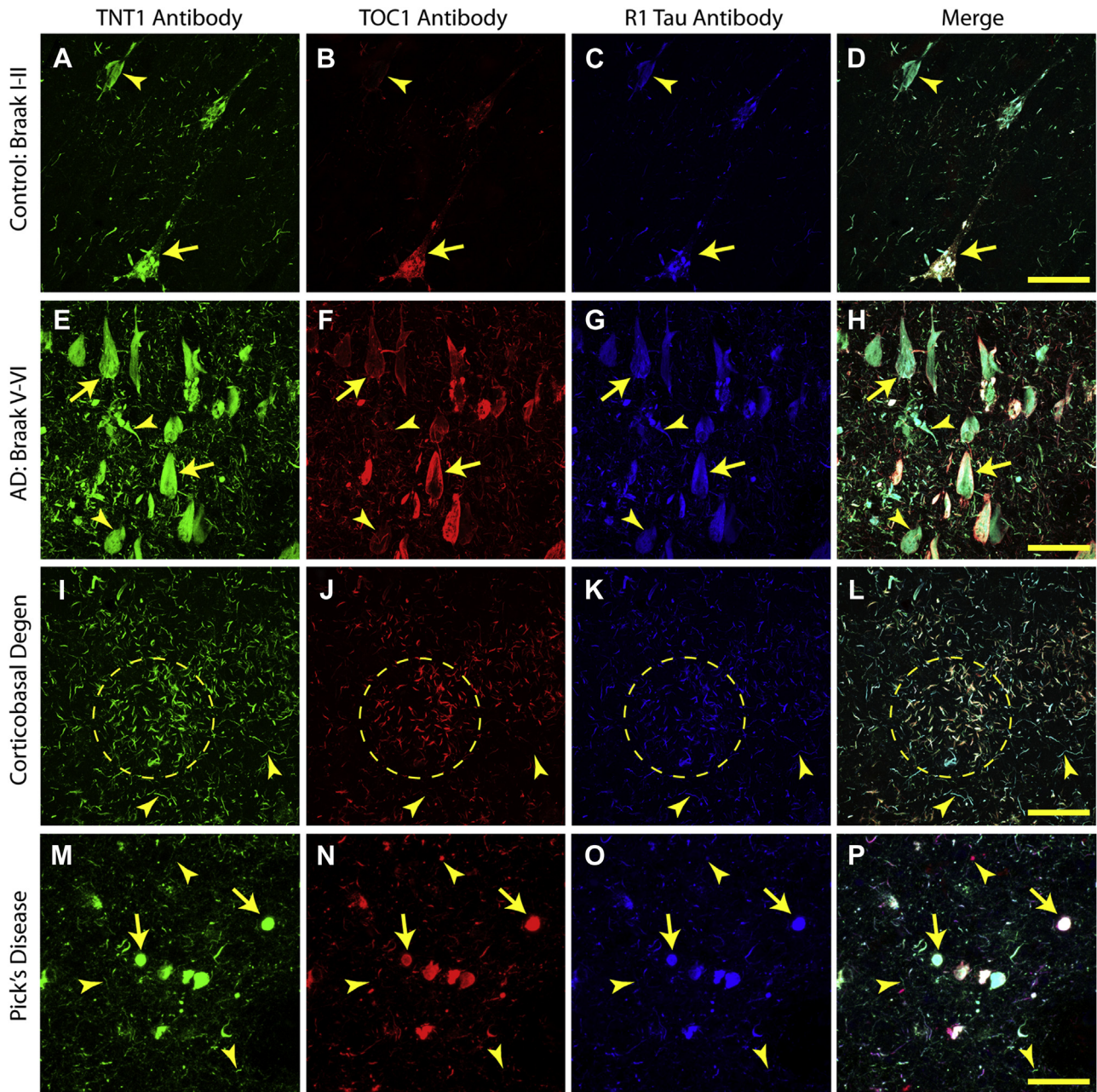
Fig. 5. PAD exposure and tau oligomer formation occur simultaneously in the pathognomonic pathology of Alzheimer's disease (AD), corticobasal degeneration (CBD), and Pick's disease (PiD). (A–P) Triple-label IF for TNT1 (green), TOC1 (red), and R1 (blue) was used to determine the extent of colocalization between PAD-exposed tau (TNT1 reactivity) and tau oligomers (TOC1 reactivity), and total tau (R1 reactivity). (A–D) Staining confirmed that PAD exposure and tau oligomerization are present in the same neurons in early pretangle neurons (arrow) in nondemented Braak stage I–II cases. Despite a high degree of overlap between TNT1 and TOC1, occasional inclusions were TNT1 reactive but lacked TOC1 reactivity (arrowheads). (E–H) Both PAD-exposed tau and tau oligomers remain highly colocalized in late AD brains (Braak stage V–VI, arrow) with both markers continuing to label classic neurofibrillary tangles. It is notable that occasional inclusions do not show strong colocalization between TNT1 and TOC1 (arrowheads) suggesting that these events are not always concurrent. (I–L) PAD exposure and tau oligomerization are present in the astrocytic inclusions characteristic of CBD in the frontal cortex (glial plaque identified with dashed outline). Again, some discrete glial threads appeared to contain a low level of TNT1 and TOC1 colocalization (arrowheads) indicating that PAD exposure and oligomerization are not always linked in CBD. (M–P) Pick bodies show robust labeling and colocalization with TNT1 and TOC1 in the frontal cortex of PiD brains (arrows). Occasionally, some inclusions were not double stained with TNT1 and TOC1 (arrowheads) suggesting that in PiD these modifications are not always codistributed. All scale bars are 50 μm. Abbreviation: PAD, phosphatase-activating domain. (For interpretation of the references to color in this figure legend, the reader is referred to the Web version of this article.)

4. Discussion

The involvement of different tau isoforms in several unrelated tauopathies is well established, but mechanisms linking different isoforms to cell degeneration have not been established. Based on our prior work, we set out to establish the extent of oligomer formation (as measured by TOC1 immunoreactivity [Patterson et al., 2011a; Ward et al., 2013]) and conformational display of PAD (as measured by TNT1 reactivity [Kanaan et al., 2011, 2012]) in aggregates composed of each human tau isoform. In addition, we tested whether tau aggregates of each isoform are toxic to FAT in the squid axoplasm assay (Song et al., 2016). Results from biochemical assays indicated that aggregation increased oligomer formation and PAD exposure for all tau isoforms. The degree of these conformational
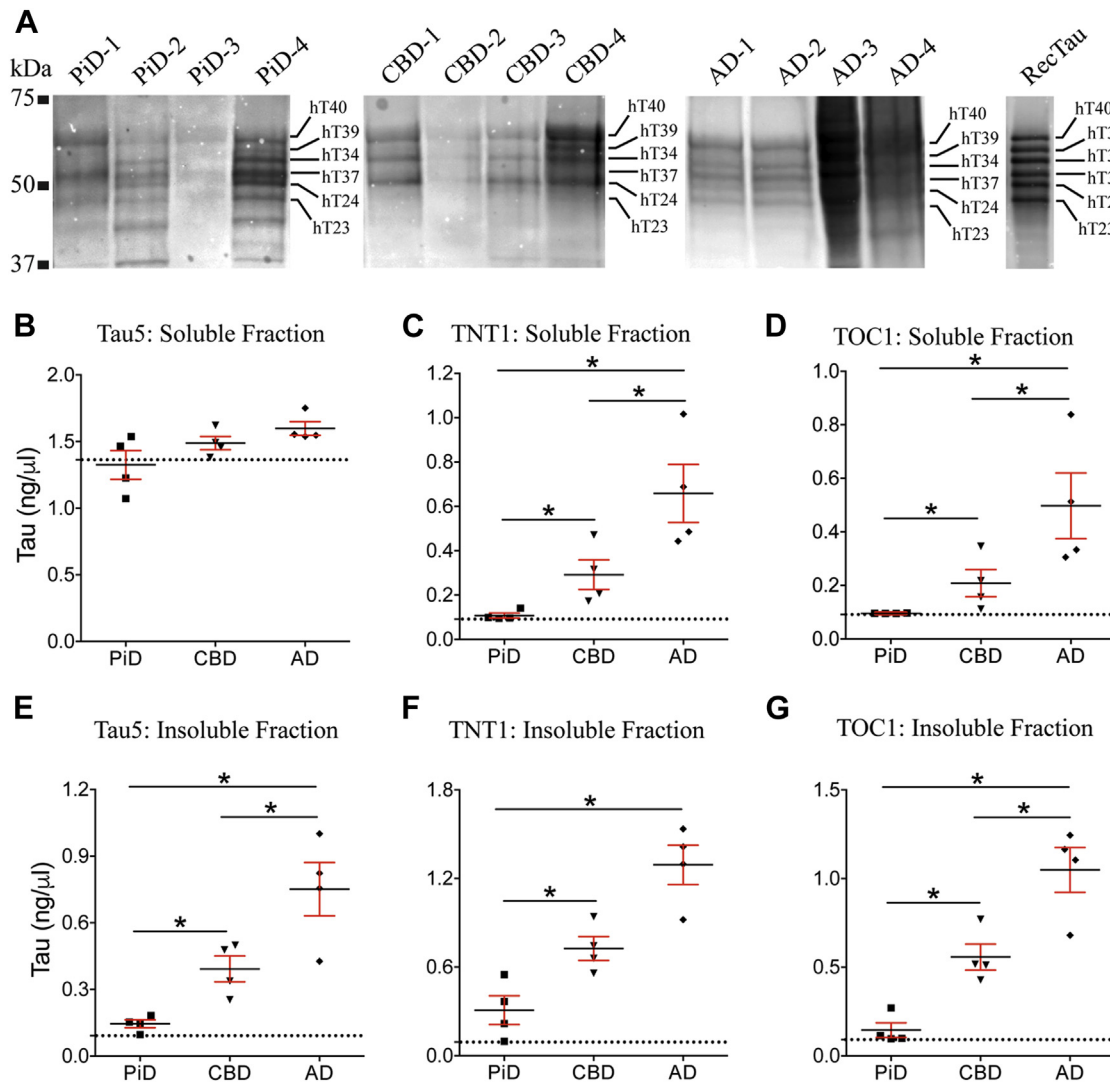
Fig. 6. Immunochemical analysis of tau isoforms, PAD exposure and oligomerization in the frontal cortex of PiD, CBD, and AD brains. (A) Immunoblots of the dephosphorylated, sarkosyl-insoluble tau fractions from the AD, PiD, and CBD cases displaying the isoform composition. AD cases show a mixture of isoforms, the PiD cases clearly contain 3R isoforms, but also some 4R isoforms, while the vast majority of pathology in CBD cases 4R tau isoforms. A recombinant protein (Rec Tau) standard containing all 6 tau isoforms was run to confirm each isoform band. (B–D) Sandwich ELISAs were used to quantify the level of total tau (B, Tau5 capture), PAD-exposed tau (C, TNT1 capture), or tau oligomers (D, TOC1 capture) in soluble protein fractions. (B) As expected, the soluble fraction contained equal levels of tau proteins in all groups. (C, D) The level of PAD-exposed tau (C) and oligomeric tau (D) was the highest in AD cases, followed CBD cases, and the lowest level among the tauopathies was in PiD. The dashed lined represents the average signal from ND control cases and is included as a reference point for "normal" levels in all graphs. (E–G) Sandwich ELISAs were also used to quantify the level of total tau (E, Tau5 capture), PAD-exposed tau (F, TNT1 capture), or tau oligomers (G, TOC1 capture) in the sarkosyl-insoluble fractions. (E) The sarkosyl-insoluble fraction contained significantly more total tau in AD compared to CBD and PiD, and CBD had more than PiD. (F) Significantly more PAD-exposed tau was found in AD and CBD when compared with PiD. (G) The amount of oligomeric tau proteins in AD was the highest, and CBD cases contained were significantly higher levels compared with PiD. ELISA values represent the average level of tau (ng/μL) ± SEM (n = 4 per group), and the data were compared using a 1-way ANOVA with Holm–Sidak post-hoc test ($*p < 0.05$). Abbreviations: AD, Alzheimer's disease; ANOVA, analysis of variance; CBD, corticobasal degeneration; ELISA, enzyme-linked immunosorbent assays; PAD, phosphatase-activating domain; PiD, Pick's disease; SEM, standard error of mean.

changes was greater for 4R isoform aggregates, when compared to 3R isoforms. Most important, aggregates of all 6 isoforms significantly impaired anterograde FAT, thus extending prior findings from experiments using the longest 4R tau isoform (Kanaan et al., 2011, 2012; LaPointe et al., 2009). Although the longest 3R isoform (hT39) was found to impair retrograde FAT slightly, a finding not seen with any other unmodified tau construct evaluated to date (Kanaan et al., 2011, 2012; LaPointe et al., 2009; Morfini et al., 2007; Patterson et al., 2011a), and while this may be due to a slight increase in retrograde rates with monomeric hT39, we recently found that pseudophosphorylated Ser 422 tau aggregates also impair retrograde FAT through an unknown mechanism (Tiernan et al., 2016). Either way, this is intriguing and may merit further characterization. Highlighting the relevance of these observations to

human disease, we showed oligomer formation and PAD exposure occur in multiple tauopathies (i.e., AD, CBD, and PiD) that involve various combinations of the tau isoforms.

4.1. PAD exposure and oligomer formation in human tau isoforms

Conformational changes in the tau protein are considered to be exceptionally important in the formation of pathological inclusions and toxic effects of tau proteins in human tauopathies. Pathological conformations thought to facilitate the aggregation of tau were originally identified when conformation-specific antibodies, such as Alz50 and MC1, were characterized as having discontinuous epitopes (Carmel et al., 1996; Hyman et al., 1988; Jicha et al., 1997, 1999). The recent development of tau antibodies that detect PAD

exposure (Combs et al., 2016; Kanaan et al., 2011) or oligomeric species (Castillo-Carranza et al., 2014b; Lasagna-Reeves et al., 2012; Patterson et al., 2011a; Ward et al., 2013) has facilitated additional insight into the pathological conformations adopted by tau. More recently, we showed that several disease-related modifications of tau cause conformational display of the PAD in the amino terminus of tau and oligomeric tau aggregates impaired axonal transport confirming a link between pathological conformations and tau toxicity (Kanaan et al., 2011; LaPointe et al., 2009; Patterson et al., 2011a, b; Tiernan et al., 2016). Moreover, many other studies suggest oligomeric tau is toxic to neurons in culture and in vivo (Castillo-Carranza et al., 2014a, b; Fa et al., 2016; Gerson et al., 2016; Lasagna-Reeves et al., 2010; Tian et al., 2013; Usenovic et al., 2015). Previous studies have focused only on the longest 4R tau isoform to study the effects of PAD exposure and oligomerization. Here, we extended those studies to all 6 human tau isoforms in the central nervous system. Despite some differences in the morphology of aggregates, PAD exposure and oligomerization occurred with all 6 human tau isoforms when aggregated in vitro.

The measurements of aggregation for each isoform are in general agreement with previous studies assessing tau isoform aggregation with ARA-induced polymerization (Combs et al., 2011; King et al., 2000; Voss and Gamblin, 2009). Visual inspection of the aggregates using electron microscopy showed that the morphology of aggregates with different isoforms were quite distinct. Our data further support this conclusion by showing that there are differences in the reactivity with conformation-dependent antibodies (TNT1 and TOC1) among the recombinant tau isoform aggregates and tauopathy aggregates. Our recombinant protein data showed greater reactivity with both TNT1 and TOC1 for the 4R isoforms compared to 3R isoforms, and the shortest 4R isoforms showed the greatest signal among the 4R proteins, while the opposite was true for 3R isoforms. We confirmed that the differences in TNT1 and TOC1 reactivity were dependent on conformation because when the samples are assayed under denaturing conditions equal reactivity was observed. The varying levels of reactivity for TNT1 and TOC1 and obvious morphological difference among tau isoform aggregates suggest that there are likely structural differences not identified by electron microscopy. Moreover, there appears to be a relationship between TNT1 and TOC1 reactivity in nondenaturing assays with the tau isoform aggregates, although it is likely that a single monoclonal antibody may not be able to equally detect all conformational structures associated with different tau species, as previously suggested for other oligomeric antibodies (Kayed et al., 2010; Rasool et al., 2013).

Interestingly, the ultrastructural morphology of tau filaments in the tauopathies display some distinct features (Crowther, 1990; Crowther and Goedert, 2000) that suggest structural differences exist between aggregates composed of different tau isoforms in human disease. Our data support this conclusion because, while PAD exposure and oligomer formation were observed in AD (4R and 3R pathology), CBD (4R pathology), and PiD (3R pathology), the extent of signal was the lowest in PiD in the biochemical assays. Interestingly, the fact that our human PiD cases contained some 4R isoforms suggests that these potential structural differences may not be entirely isoform-specific but are also dependent on still unknown disease-specific factors. The presence of PAD exposure and oligomerization in all of these tauopathies is further supported by the extensive colocalization observed between TNT1 and TOC1 in AD, CBD, and PiD. The diversity of tau inclusions suggests that different processes may dictate the formation of tau inclusions in each tauopathy, but unfortunately, these mechanisms remain unidentified. Nonetheless, oligomer formation and PAD exposure may elicit toxicity to transport in all of these tauopathies.

It is important to note that the fixation and staining methods used in the human tissue studies here should leave tau conformations intact allowing TNT1 and TOC1 to label the pathological conformations. Previous studies suggest that formaldehyde fixation does not significantly alter secondary and tertiary conformations in proteins (Mason and O'Leary, 1991; Rait et al., 2004). We have recently shown that N-terminal tau antibodies (e.g., Tau13 and Tau12) with epitopes immediately downstream of TNT1 robustly label parenchymal tau (i.e., normal tau) as well as tau inclusions demonstrating that they do not distinguish between normal and pathological tau conformations in tissue sections (Combs et al., 2016). In contrast, TNT1 and TOC1 are specific to pathological inclusions and do not label parenchymal tau, further suggesting that conformational differences remain in fixed human tissue samples (Combs et al., 2016; Kanaan et al., 2011; Patterson et al., 2011a; Ward et al., 2013).

The hT39 monomers showed a significant increase in TNT1 and TOC1 reactivity unlike other 3R isoform monomers. Perhaps, this signifies inherent structural or folding differences in the longest 3R isoform compared with other isoforms. It is also noteworthy that a nonsignificant increase in TNT1 and TOC1 reactivity was also observed with hT40 monomers, again suggesting the longest 4R isoform may exhibit a greater tendency for TNT1 and TOC1 epitope display. There is clear evidence that several tau conformations can form dynamically, and it seems likely that the protein may normally shift between folded global conformations and "unfolded" states as a soluble monomer (Jeganathan et al., 2008; Mukrasch et al., 2009). Thus, it is not entirely surprising that both TNT1 and TOC1 show low levels of reactivity with monomers of the longest isoforms when abundant amounts of the proteins are analyzed.

Most important, we and others have suggested that those tau post-translational modifications regulate tau folding in situ and those disease-related modifications like abnormal phosphorylation and/or aggregation may enhance aberrant PAD exposure and could prevent tau from returning to a regulatable, monomeric state. While these potential regulatory events are not well understood, phosphorylation is important in modulating tau conformations. Previous studies have shown that pseudophosphorylation at the AT8 site alters tau folding (Jeganathan et al., 2008) and significantly impairs anterograde FAT as a monomeric protein (Kanaan et al., 2011), and more recently, we found that pseudophosphorylation at Ser 422 similarly impairs anterograde transport as a monomer and is toxic to retrograde transport when aggregated (Tiernan et al., 2016). Conversely, phosphorylation of tyrosine 18 within PAD appears to mitigate the deleterious effects of pathological forms of tau (Kanaan et al., 2012) and might be involved in the normal regulation of PAD-dependent effects on transport (Kanaan et al., 2015).

4.2. A common mechanism of toxicity to all human tau isoform aggregates

Axonal transport is a cellular process critical for the maintenance of neural connectivity and impairment in transport is increasingly implicated in the pathogenesis of several neurodegenerative diseases, including tauopathies (Morfini et al., 2009). Dystrophic neurites, synaptic loss, and protein mislocalization are pathological features in tauopathies, and evidence of FAT impairments (e.g., axonal swellings, synaptic loss, and impaired vesicle transport) is present in several tauopathy animal models (Gotz et al., 2006; Kanaan et al., 2013; Morfini et al., 2009). Recently, our group described a mechanism by which physiological levels of hT40 tau with PAD exposed (e.g., aggregates and other disease-related modifications) caused inhibition of kinesin-dependent anterograde FAT (Kanaan et al., 2011; LaPointe et al., 2009). Once hT40 PAD is abnormally exposed, it triggers a PP1/GSK3 signaling

pathway that leads to kinesin phosphorylation and cargo detachment (Morfini et al., 2002, 2004). Until now, it was unclear whether other tau isoforms would similarly inhibit anterograde FAT on aggregation.

To our knowledge, this is the first report showing that aggregates of all 6 tau isoforms produced axonal transport toxicity. Interestingly, some interisoform differences were noted. Specifically, hT24 aggregates, the shortest 4R isoform, produced the most robust inhibition of anterograde FAT and showed the highest level of TNT1 and TOC1 reactivity. Based on the structural differences described previously, these findings suggest that aggregates composed of the shortest 4R tau isoform are structurally arranged to expose PAD more readily than other isoform aggregates, which would explain the increased toxicity and transport impairment. Despite such differences, it is important to emphasize that all isoform aggregates produced significant inhibition of anterograde transport. These data indicate that this PAD-dependent toxic mechanism (Kanaan et al., 2011; LaPointe et al., 2009) is relevant for multiple tauopathies irrespective of the isoforms composing the pathological inclusions.

A great deal of focus has been placed on whether monomers, oligomers, filaments, or various forms of all these tau species are toxic (Lasagna-Reeves et al., 2011; Sahara et al., 2008, 2014; Ward et al., 2012). Indeed, multiple studies implicate oligomers as a primary toxic species of tau in several tauopathy model systems (Cardenas-Aguayo Mdel et al., 2014; Castillo-Carranza et al., 2014a; Fa et al., 2016; Gerson et al., 2016; Lewis and Dickson, 2016; Sahara et al., 2013; Tian et al., 2013; Usenovic et al., 2015; Ward et al., 2012). Here, the vast majority of aggregates produced by the 3R isoforms under the experimental conditions used were oligomeric, with only rare filaments being present in the sample. These samples significantly impaired transport suggesting oligomeric species are sufficient for transport inhibition. This is consistent with previous work showing that Hsp70 binds with tau oligomers (only the hT40 isoform was studied) but not with tau filaments. Furthermore, Hsp70 blocked the deleterious effects of hT40 tau aggregates consisting of both oligomers and filaments on axonal transport suggesting that tau oligomers are responsible for the inhibitory effect (Patterson et al., 2011b). However, these studies do not rule out potential toxicity from modified monomers and/or filaments, which will require further investigation.

Another interesting difference between specific human tauopathies is the diversity of cell types that are affected and contain tau inclusions. For example, AD and PiD primarily involve neuronal inclusions (Braak et al., 2006; Delacourte et al., 1996), while other tauopathies such as PSP and CBD involve several forms of glial inclusions (Berry et al., 2004; Buee Scherrer et al., 1996; Dickson, 1999), and yet, others such as CTE are characterized by a mixture of neuronal and glial inclusions (McKee et al., 2014). Here, we provide evidence for a common tau-mediated toxic mechanism for all 6 isoforms involving impairment of microtubule-based anterograde transport (plus-end directed, kinesin-based). The role of axonal transport in maintaining neuron connectivity and survival is well established (Kevenaar and Hoogenraad, 2015; Maday et al., 2014), and the importance of microtubule-based transport extends to both the somatodendritic compartment and glial cells (Baas et al., 2016; Kreft et al., 2009). Indeed, microtubule-based transport is widely involved in intracellular trafficking for several cellular components including trafficking of myelin components in oligodendrocytes (Carson et al., 1997; Lyons et al., 2009). Moreover, tau-induced astrocyte toxicity was associated with impaired kinesin-dependent transport (Yoshiyama et al., 2003). Thus, the findings here may have implications for potential mechanisms of toxicity within both neurons and glial cells in tauopathies of unrelated etiology.

5. Conclusions

The diversity in human tauopathy diseases is poorly understood, but one central difference is the isoform composition of the pathognomonic inclusions. Until now, the identity of common features that would explain how each isoform contributes to disease pathogenesis remained unknown. However, our data suggest a model where aggregation-dependent PAD exposure and transport inhibition represent a common toxic mechanism relevant to all human tau isoforms. Under this model, cell type-specific differences in tau isoform expression and aggregation may explain at least in part the differential vulnerability of cells observed in different tauopathies. These findings provide a novel mechanistic basis linking the aggregation process in all tau isoforms to a specific conformational change (i.e., PAD exposure) and a common toxic effect on transport and other cell processes affected by PP1/GSK3 signaling. This provides a basis for the development of novel therapeutic strategies for all tauopathies based on blocking or reducing PAD exposure.

Supplementary data

Supplementary data related to this article can be found at http://dx.doi.org/10.1016/j.neurobiolaging.2016.07.015.

References

Adams, S.J., DeTure, M.A., McBride, M., Dickson, D.W., Petrucelli, L., 2010. Three repeat isoforms of tau inhibit assembly of four repeat tau filaments. PLoS One 5, e10810.

Alonso, A.C., Grundke-Iqbal, I., Iqbal, K., 1996. Alzheimer's disease hyperphosphorylated tau sequesters normal tau into tangles of filaments and disassembles microtubules. Nat. Med. 2, 783–787.

Baas, P.W., Rao, A.N., Matamoros, A.J., Leo, L., 2016. Stability properties of neuronal microtubules. Cytoskeleton.

Berry, R.W., Sweet, A.P., Clark, F.A., Lagalwar, S., Lapin, B.R., Wang, T., Topgi, S., Guillozet-Bongaarts, A.L., Cochran, E.J., Bigio, E.H., Binder, L.I., 2004. Tau epitope display in progressive supranuclear palsy and corticobasal degeneration. J. Neurocytol. 33, 287–295.

Boutajangout, A., Boom, A., Leroy, K., Brion, J.P., 2004. Expression of tau mRNA and soluble tau isoforms in affected and non-affected brain areas in Alzheimer's disease. FEBS Lett. 576, 183–189.

Braak, H., Alafuzoff, I., Arzberger, T., Kretzschmar, H., Del Tredici, K., 2006. Staging of Alzheimer disease-associated neurofibrillary pathology using paraffin sections and immunocytochemistry. Acta Neuropathol. 112, 389–404.

Buee, L., Delacourte, A., 1999. Comparative biochemistry of tau in progressive supranuclear palsy, corticobasal degeneration, FTDP-17 and Pick's disease. Brain Pathol. 9, 681—693.

Buee Scherrer, V., Hof, P.R., Buee, L., Leveugle, B., Vermersch, P., Perl, D.P., Olanow, C.W., Delacourte, A., 1996. Hyperphosphorylated tau proteins differentiate corticobasal degeneration and Pick's disease. Acta Neuropathol. 91, 351—359.

Bunker, J.M., Wilson, L., Jordan, M.A., Feinstein, S.C., 2004. Modulation of microtubule dynamics by tau in living cells: implications for development and neurodegeneration. Mol. Biol. Cell 15, 2720—2728.

Butner, K.A., Kirschner, M.W., 1991. Tau protein binds to microtubules through a flexible array of distributed weak sites. J. Cell Biol. 115, 717—730.

Cardenas-Aguayo Mdel, C., Gomez-Virgilio, L., DeRosa, S., Meraz-Rios, M.A., 2014. The role of tau oligomers in the onset of Alzheimer's disease neuropathology. ACS Chem. Neurosci. 5, 1178—1191.

Carmel, G., Leichus, B., Cheng, X., Patterson, S.D., Mirza, U., Chait, B.T., Kuret, J., 1994. Expression, purification, crystallization, and preliminary x-ray analysis of casein kinase-1 from Schizosaccharomyces pombe. J. Biol. Chem. 269, 7304—7309.

Carmel, G., Mager, E.M., Binder, L.I., Kuret, J., 1996. The structural basis of monoclonal antibody Alz50's selectivity for Alzheimer's disease pathology. J. Biol. Chem. 271, 32789—32795.

Carson, J.H., Worboys, K., Ainger, K., Barbarese, E., 1997. Translocation of myelin basic protein mRNA in oligodendrocytes requires microtubules and kinesin. Cell Motil. Cytoskeleton 38, 318—328.

Castillo-Carranza, D.L., Gerson, J.E., Sengupta, U., Guerrero-Munoz, M.J., Lasagna-Reeves, C.A., Kayed, R., 2014a. Specific targeting of tau oligomers in Htau mice prevents cognitive impairment and tau toxicity following injection with brain-derived tau oligomeric seeds. J. Alzheimers Dis. 40, S97—s111.

Castillo-Carranza, D.L., Sengupta, U., Guerrero-Munoz, M.J., Lasagna-Reeves, C.A., Gerson, J.E., Singh, G., Estes, D.M., Barrett, A.D., Dineley, K.T., Jackson, G.R., Kayed, R., 2014b. Passive immunization with Tau oligomer monoclonal antibody reverses tauopathy phenotypes without affecting hyperphosphorylated neurofibrillary tangles. J. Neurosci. 34, 4260—4272.

Chen, J., Kanai, Y., Cowan, N.J., Hirokawa, N., 1992. Projection domains of MAP2 and tau determine spacings between microtubules in dendrites and axons. Nature 360, 674—677.

Combs, B., Hamel, C., Kanaan, N.M., 2016. Pathological conformations involving the amino terminus of tau occur early in Alzheimer's disease and are differentially detected by monoclonal antibodies. Neurobiol. Dis. 94, 18—31.

Combs, B., Voss, K., Gamblin, T.C., 2011. Pseudohyperphosphorylation has differential effects on polymerization and function of tau isoforms. Biochemistry 50, 9446—9456.

Crowther, R.A., 1990. Structural aspects of pathology in Alzheimer's disease. Biochim. Biophys. Acta 1096, 1—9.

Crowther, R.A., Goedert, M., 2000. Abnormal tau-containing filaments in neurodegenerative diseases. J. Struct. Biol. 130, 271—279.

Delacourte, A., Robitaille, Y., Sergeant, N., Buee, L., Hof, P.R., Wattez, A., Laroche-Cholette, A., Mathieu, J., Chagnon, P., Gauvreau, D., 1996. Specific pathological Tau protein variants characterize Pick's disease. J. Neuropathol. Exp. Neurol. 55, 159—168.

Dickson, D.W., 1999. Neuropathologic differentiation of progressive supranuclear palsy and corticobasal degeneration. J. Neurol. 246, II6—II15.

Fa, M., Puzzo, D., Piacentini, R., Staniszewski, A., Zhang, H., Baltrons, M.A., Li Puma, D.D., Chatterjee, I., Li, J., Saeed, F., Berman, H.L., Ripoli, C., Gulisano, W., Gonzalez, J., Tian, H., Costa, J.A., Lopez, P., Davidowitz, E., Yu, W.H., Haroutunian, V., Brown, L.M., Palmeri, A., Sigurdsson, E.M., Duff, K.E., Teich, A.F., Honig, L.S., Sierks, M., Moe, J.G., D'Adamio, L., Grassi, C., Kanaan, N.M., Fraser, P.E., Arancio, O., 2016. Extracellular tau oligomers produce an immediate impairment of LTP and memory. Sci. Rep. 6, 19393.

Ferrer, I., Lopez-Gonzalez, I., Carmona, M., Arregui, L., Dalfo, E., Torrejon-Escribano, B., Diehl, R., Kovacs, G.G., 2014. Glial and neuronal tau pathology in tauopathies: characterization of disease-specific phenotypes and tau pathology progression. J. Neuropathol. Exp. Neurol. 73, 81—97.

Gamblin, T.C., King, M.E., Dawson, H., Vitek, M.P., Kuret, J., Berry, R.W., Binder, L.I., 2000. In vitro polymerization of tau protein monitored by laser light scattering: method and application to the study of FTDP-17 mutants. Biochemistry 39, 6136—6144.

Gerson, J.E., Castillo-Carranza, D.L., Sengupta, U., Bodani, R., Prough, D.S., DeWitt, D., Hawkins, B.E., Kayed, R., 2016. Tau oligomers derived from Traumatic Brain Injury cause cognitive impairment and accelerate onset of pathology in Htau mice. J. Neurotrauma [Epub ahead of print].

Goedert, M., Jakes, R., 1990. Expression of separate isoforms of human tau protein: correlation with the tau pattern in brain and effects on tubulin polymerization. EMBO J. 9, 4225—4230.

Goedert, M., Spillantini, M.G., Cairns, N.J., Crowther, R.A., 1992. Tau proteins of Alzheimer paired helical filaments: abnormal phosphorylation of all six brain isoforms. Neuron 8, 159—168.

Gotz, J., Ittner, L.M., Kins, S., 2006. Do axonal defects in tau and amyloid precursor protein transgenic animals model axonopathy in Alzheimer's disease? J. Neurochem. 98, 993—1006.

Hong, M., Zhukareva, V., Vogelsberg-Ragaglia, V., Wszolek, Z., Reed, L., Miller, B.I., Geschwind, D.H., Bird, T.D., McKeel, D., Goate, A., Morris, J.C., Wilhelmsen, K.C., Schellenberg, G.D., Trojanowski, J.Q., Lee, V.M., 1998. Mutation-specific functional impairments in distinct tau isoforms of hereditary FTDP-17. Science (New York, NY) 282, 1914—1917.

Horowitz, P.M., LaPointe, N., Guillozet-Bongaarts, A.L., Berry, R.W., Binder, L.I., 2006. N-terminal fragments of tau inhibit full-length tau polymerization in vitro. Biochemistry 45, 12859—12866.

Hyman, B.T., Van Hoesen, G.W., Wolozin, B.L., Davies, P., Kromer, L.J., Damasio, A.R., 1988. Alz-50 antibody recognizes Alzheimer-related neuronal changes. Ann. Neurol. 23, 371—379.

Jeganathan, S., Hascher, A., Chinnathambi, S., Biernat, J., Mandelkow, E.M., Mandelkow, E., 2008. Proline-directed pseudo-phosphorylation at AT8 and PHF1 epitopes induces a compaction of the paperclip folding of Tau and generates a pathological (MC-1) conformation. J. Biol. Chem. 283, 32066—32076.

Jicha, G.A., Bowser, R., Kazam, I.G., Davies, P., 1997. Alz-50 and MC-1, a new monoclonal antibody raised to paired helical filaments, recognize conformational epitopes on recombinant tau. J. Neurosci. Res. 48, 128—132.

Jicha, G.A., Berenfeld, B., Davies, P., 1999. Sequence requirements for formation of conformational variants of tau similar to those found in Alzheimer's disease. J. Neurosci. Res. 55, 713—723.

Kanaan, N.M., Morfini, G.A., LaPointe, N.E., Pigino, G.F., Patterson, K.R., Song, Y., Andreadis, A., Fu, Y., Brady, S.T., Binder, L.I., 2011. Pathogenic forms of tau inhibit kinesin-dependent axonal transport through a mechanism involving activation of axonal phosphotransferases. J. Neurosci. 31, 9858—9868.

Kanaan, N.M., Morfini, G., Pigino, G., LaPointe, N.E., Andreadis, A., Song, Y., Leitman, E., Binder, L.I., Brady, S.T., 2012. Phosphorylation in the amino terminus of tau prevents inhibition of anterograde axonal transport. Neurobiol. Aging 33, 826.e15—826.e30.

Kanaan, N.M., Cox, K., Alvarez, V.E., Stein, T.D., Poncil, S., McKee, A.C., 2016. Characterization of early pathological tau conformations and phosphorylation in chronic traumatic encephalopathy. J. Neuropathol. Exp. Neurol. 75, 19—34.

Kanaan, N.M., Himmelstein, D.S., Ward, S.M., Combs, B., Binder, L.I., 2015. Tau protein: biology and pathobiology. In: LeDoux, M.S. (Ed.), Movement Disorders: Genetics and Models. Burlington, MA: Elsevier, pp. 857—874.

Kanaan, N.M., Pigino, G.F., Brady, S.T., Lazarov, O., Binder, L.I., Morfini, G.A., 2013. Axonal degeneration in Alzheimer's disease: when signaling abnormalities meet the axonal transport system. Exp. Neurol. 246, 44—53.

Kanai, Y., Takemura, R., Oshima, T., Mori, H., Ihara, Y., Yanagisawa, M., Masaki, T., Hirokawa, N., 1989. Expression of multiple tau isoforms and microtubule bundle formation in fibroblasts transfected with a single tau cDNA. J. Cell Biol. 109, 1173—1184.

Kayed, R., Canto, I., Breydo, L., Rasool, S., Lukacsovich, T., Wu, J., Albay 3rd, R., Pensalfini, A., Yeung, S., Head, E., Marsh, J.L., Glabe, C., 2010. Conformation dependent monoclonal antibodies distinguish different replicating strains or conformers of prefibrillar Abeta oligomers. Mol. Neurodegener. 5, 57.

Kevenaar, J.T., Hoogenraad, C.C., 2015. The axonal cytoskeleton: from organization to function. Front Mol. Neurosci. 8, 44.

King, M.E., Ahuja, V., Binder, L.I., Kuret, J., 1999. Ligand-dependent tau filament formation: implications for Alzheimer's disease progression. Biochemistry 38, 14851—14859.

King, M.E., Gamblin, T.C., Kuret, J., Binder, L.I., 2000. Differential assembly of human tau isoforms in the presence of arachidonic acid. J. Neurochem. 74, 1749—1757.

Kovacs, G.G., 2015. Invited review: neuropathology of tauopathies: principles and practice. Neuropathol. Appl. Neurobiol. 41, 3—23.

Kreft, M., Potokar, M., Stenovec, M., Pangrsic, T., Zorec, R., 2009. Regulated exocytosis and vesicle trafficking in astrocytes. Ann. N. Y. Acad. Sci. 1152, 30—42.

LaPointe, N.E., Morfini, G., Pigino, G., Gaisina, I.N., Kozikowski, A.P., Binder, L.I., Brady, S.T., 2009. The amino terminus of tau inhibits kinesin-dependent axonal transport: implications for filament toxicity. J. Neurosci. Res. 87, 440—451.

Lasagna-Reeves, C.A., Castillo-Carranza, D.L., Guerrero-Muoz, M.J., Jackson, G.R., Kayed, R., 2010. Preparation and characterization of neurotoxic tau oligomers. Biochemistry 49, 10039—10041.

Lasagna-Reeves, C.A., Castillo-Carranza, D.L., Jackson, G.R., Kayed, R., 2011. Tau oligomers as potential targets for immunotherapy for Alzheimer's disease and tauopathies. Curr. Alzheimer Res. 8, 659—665.

Lasagna-Reeves, C.A., Castillo-Carranza, D.L., Sengupta, U., Sarmiento, J., Troncoso, J., Jackson, G.R., Kayed, R., 2012. Identification of oligomers at early stages of tau aggregation in Alzheimer's disease. FASEB J. 26, 1946—1959.

Levy, S.F., Leboeuf, A.C., Massie, M.R., Jordan, M.A., Wilson, L., Feinstein, S.C., 2005. Three- and four-repeat tau regulate the dynamic instability of two distinct microtubule subpopulations in qualitatively different manners. Implications for neurodegeneration. J. Biol. Chem. 280, 13520—13528.

Lewis, J., Dickson, D.W., 2016. Propagation of tau pathology: hypotheses, discoveries, and yet unresolved questions from experimental and human brain studies. Acta Neuropathol. 131, 27—48.

Litersky, J.M., Scott, C.W., Johnson, G.V., 1993. Phosphorylation, calpain proteolysis and tubulin binding of recombinant human tau isoforms. Brain Res. 604, 32—40.

Lyons, D.A., Naylor, S.G., Scholze, A., Talbot, W.S., 2009. Kif1b is essential for mRNA localization in oligodendrocytes and development of myelinated axons. Nat. Genet. 41, 854—858.

Maday, S., Twelvetrees, A.E., Moughamian, A.J., Holzbaur, E.L., 2014. Axonal transport: cargo-specific mechanisms of motility and regulation. Neuron 84, 292—309.

Mason, J.T., O'Leary, T.J., 1991. Effects of formaldehyde fixation on protein secondary structure: a calorimetric and infrared spectroscopic investigation. J. Histochem. Cytochem. 39, 225—229.

McKee, A.C., Daneshvar, D.H., Alvarez, V.E., Stein, T.D., 2014. The neuropathology of sport. Acta Neuropathol. 127, 29—51.

McKee, A.C., Stern, R.A., Nowinski, C.J., Stein, T.D., Alvarez, V.E., Daneshvar, D.H., Lee, H.S., Wojtowicz, S.M., Hall, G., Baugh, C.M., Riley, D.O., Kubilus, C.A., Cormier, K.A., Jacobs, M.A., Martin, B.R., Abraham, C.R., Ikezu, T., Reichard, R.R., Wolozin, B.L., Budson, A.E., Goldstein, L.E., Kowall, N.W., Cantu, R.C., 2013. The spectrum of disease in chronic traumatic encephalopathy. Brain 136, 43—64.

Morfini, G., Szebenyi, G., Brown, H., Pant, H.C., Pigino, G., DeBoer, S., Beffert, U., Brady, S.T., 2004. A novel CDK5-dependent pathway for regulating GSK3 activity and kinesin-driven motility in neurons. EMBO J. 23, 2235—2245.

Morfini, G., Pigino, G., Mizuno, N., Kikkawa, M., Brady, S.T., 2007. Tau binding to microtubules does not directly affect microtubule-based vesicle motility. J. Neurosci. Res. 85, 2620—2630.

Morfini, G., Szebenyi, G., Elluru, R., Ratner, N., Brady, S.T., 2002. Glycogen synthase kinase 3 phosphorylates kinesin light chains and negatively regulates kinesin-based motility. EMBO J. 21, 281—293.

Morfini, G.A., Burns, M., Binder, L.I., Kanaan, N.M., LaPointe, N., Bosco, D.A., Brown Jr., R.H., Brown, H., Tiwari, A., Hayward, L., Edgar, J., Nave, K.A., Garberrn, J., Atagi, Y., Song, Y., Pigino, G., Brady, S.T., 2009. Axonal transport defects in neurodegenerative diseases. J. Neurosci. 29, 12776—12786.

Mukrasch, M.D., Bibow, S., Korukottu, J., Jeganathan, S., Biernat, J., Griesinger, C., Mandelkow, E., Zweckstetter, M., 2009. Structural polymorphism of 441-residue tau at single residue resolution. PLoS Biol. 7, e34.

Munoz, D.G., Dickson, D.W., Bergeron, C., Mackenzie, I.R., Delacourte, A., Zhukareva, V., 2003. The neuropathology and biochemistry of frontotemporal dementia. Ann. Neurol. 54, S24—S28.

Panda, D., Samuel, J.C., Massie, M., Feinstein, S.C., Wilson, L., 2003. Differential regulation of microtubule dynamics by three- and four-repeat tau: implications for the onset of neurodegenerative disease. Proc. Natl. Acad. Sci. U. S. A. 100, 9548—9553.

Patterson, K.R., Remmers, C., Fu, Y., Brooker, S., Kanaan, N.M., Vana, L., Ward, S., Reyes, J.F., Philibert, K., Glucksman, M.J., Binder, L.I., 2011a. Characterization of prefibrillar Tau oligomers in vitro and in Alzheimer disease. J. Biol. Chem. 286, 23063—23076.

Patterson, K.R., Ward, S.M., Combs, B., Voss, K., Kanaan, N.M., Morfini, G., Brady, S.T., Gamblin, T.C., Binder, L.I., 2011b. Heat shock protein 70 prevents both tau aggregation and the inhibitory effects of preexisting tau aggregates on fast axonal transport. Biochemistry 50, 10300—10310.

Rait, V.K., O'Leary, T.J., Mason, J.T., 2004. Modeling formalin fixation and antigen retrieval with bovine pancreatic ribonuclease A: I-structural and functional alterations. Lab. Invest. 84, 292—299.

Rasool, S., Martinez-Coria, H., Milton, S., Glabe, C.G., 2013. Nonhuman amyloid oligomer epitope reduces Alzheimer's-like neuropathology in 3xTg-AD transgenic mice. Mol. Neurobiol. 48, 931—940.

Sahara, N., DeTure, M., Ren, Y., Ebrahim, A.S., Kang, D., Knight, J., Volbracht, C., Pedersen, J.T., Dickson, D.W., Yen, S.H., Lewis, J., 2013. Characteristics of TBS-extractable hyperphosphorylated tau species: aggregation intermediates in rTg4510 mouse brain. J. Alzheimers Dis. 33, 249—263.

Sahara, N., Maeda, S., Takashima, A., 2008. Tau oligomerization: a role for tau aggregation intermediates linked to neurodegeneration. Curr. Alzheimer Res. 5, 591—598.

Sahara, N., Ren, Y., Ward, S., Binder, L.I., Suhara, T., Higuchi, M., 2014. Tau oligomers as potential targets for early diagnosis of tauopathy. J. Alzheimers Dis. 40, S91—S96.

Sarthy, J., Gamblin, T.C., 2006. A light scattering assay for arachidonic acid-induced tau fibrillization without interfering micellization. Anal. Biochem. 353, 150—152.

Scott, C.W., Blowers, D.P., Barth, P.T., Lo, M.M., Salama, A.I., Caputo, C.B., 1991. Differences in the abilities of human tau isoforms to promote microtubule assembly. J. Neurosci. Res. 30, 154—162.

Scott, C.W., Klika, A.B., Lo, M.M., Norris, T.E., Caputo, C.B., 1992. Tau protein induces bundling of microtubules in vitro: comparison of different tau isoforms and a tau protein fragment. J. Neurosci. Res. 33, 19—29.

Sergeant, N., Wattez, A., Delacourte, A., 1999. Neurofibrillary degeneration in progressive supranuclear palsy and corticobasal degeneration: tau pathologies with exclusively "exon 10" isoforms. J. Neurochem. 72, 1243—1249.

Song, Y., Kang, M., Morfini, G., Brady, S.T., 2016. Fast axonal transport in isolated axoplasm from the squid giant axon. Methods Cell Biol. 131, 331—348.

Spillantini, M.G., Goedert, M., 2013. Tau pathology and neurodegeneration. Lancet Neurol. 12, 609—622.

Tian, H., Davidowitz, E., Lopez, P., Emadi, S., Moe, J., Sierks, M., 2013. Trimeric tau is toxic to human neuronal cells at low nanomolar concentrations. Int. J. Cell Biol. 2013, 260787.

Tiernan, C.T., Combs, B., Cox, K., Morfini, G., Brady, S.T., Counts, S.E., Kanaan, N.M., 2016. Pseudophosphorylation of tau at S422 enhances SDS-stable dimer formation and impairs both anterograde and retrograde fast axonal transport. Exp. Neurol. 283, 318—329.

Trinczek, B., Biernat, J., Baumann, K., Mandelkow, E.M., Mandelkow, E., 1995. Domains of tau protein, differential phosphorylation, and dynamic instability of microtubules. Mol. Biol. Cell 6, 1887—1902.

Usenovic, M., Niroomand, S., Drolet, R.E., Yao, L., Gaspar, R.C., Hatcher, N.G., Schachter, J., Renger, J.J., Parmentier-Batteur, S., 2015. Internalized tau oligomers cause neurodegeneration by inducing accumulation of pathogenic tau in human neurons derived from induced pluripotent stem cells. J. Neurosci. 35, 14234—14250.

Voss, K., Gamblin, T.C., 2009. GSK-3beta phosphorylation of functionally distinct tau isoforms has differential, but mild effects. Mol. Neurodegener. 4, 18.

Wang, Y., Mandelkow, E., 2016. Tau in physiology and pathology. Nat. Rev. Neurosci. 17, 22—35.

Ward, S.M., Himmelstein, D.S., Lancia, J.K., Binder, L.I., 2012. Tau oligomers and tau toxicity in neurodegenerative disease. Biochem. Soc. Trans. 40, 667—671.

Ward, S.M., Himmelstein, D.S., Lancia, J.K., Fu, Y., Patterson, K.R., Binder, L.I., 2013. TOC1: characterization of a selective oligomeric tau antibody. J. Alzheimers Dis. 37, 593—602.

Yoshida, M., 2006. Cellular tau pathology and immunohistochemical study of tau isoforms in sporadic tauopathies. Neuropathology 26, 457—470.

Yoshiyama, Y., Zhang, B., Bruce, J., Trojanowski, J.Q., Lee, V.M., 2003. Reduction of detyrosinated microtubules and Golgi fragmentation are linked to tau-induced degeneration in astrocytes. J. Neurosci. 23, 10662—10671.

Zhong, Q., Congdon, E.E., Nagaraja, H.N., Kuret, J., 2012. Tau isoform composition influences rate and extent of filament formation. J. Biol. Chem. 287, 20711—20719.